

Global sensitivity analysis using derivative-based sparse Poincaré chaos expansions

Nora Lüthen¹, Olivier Roustant^{2,3}, Fabrice Gamboa³, Bertrand Iooss^{4,3}, Stefano Marelli¹, and Bruno Sudret¹

¹*Chair of Risk, Safety, and Uncertainty Quantification, ETH Zürich, 8093 Zürich, Switzerland*

²*INSA Toulouse, 135 avenue de Rangueil, 31077 Toulouse cedex 4, France*

³*Institut de Mathématiques de Toulouse, 31062 Toulouse, France*

⁴*EDF Lab Chatou, 6 Quai Watier, 78401 Chatou, France*

October 22, 2021

Abstract

Variance-based global sensitivity analysis, in particular Sobol’ analysis, is widely used for determining the importance of input variables to a computational model. Sobol’ indices can be computed cheaply based on spectral methods like polynomial chaos expansions (PCE). Another choice are the recently developed Poincaré chaos expansions (PoinCE), whose orthonormal tensor-product basis is generated from the eigenfunctions of one-dimensional Poincaré differential operators. In this paper, we show that the Poincaré basis is the unique orthonormal basis with the property that partial derivatives of the basis form again an orthogonal basis with respect to the same measure as the original basis. This special property makes PoinCE ideally suited for incorporating derivative information into the surrogate modelling process. Assuming that partial derivative evaluations of the computational model are available, we compute spectral expansions in terms of Poincaré basis functions or basis partial derivatives, respectively, by sparse regression. We show on two numerical examples that the derivative-based expansions provide accurate estimates for Sobol’ indices, even outperforming PCE in terms of bias and variance. In addition, we derive an analytical expression based on the PoinCE coefficients for a second popular sensitivity index, the derivative-based sensitivity measure (DGSM), and explore its performance as upper bound to the corresponding total Sobol’ indices.

1 Introduction

Computer models simulating physical phenomena and industrial systems are commonly used in engineering and safety studies, for prediction, validation or optimisation purposes. These numerical models often take as inputs a high number of physical parameters, whose values are variable or not perfectly known, creating the need for uncertainty quantification on model computations (Smith, 2014). Uncertainty quantification typically becomes more challenging the

higher the input dimension is (curse of dimensionality). In this situation, global sensitivity analysis (GSA) is an invaluable tool that allows the analyst to rank the relative importance of each input of the model and to detect non-influential inputs (Borgonovo and Plischke, 2016; Razavi et al., 2021). Most often relying on a probabilistic modeling of the model input variables, GSA tries to explain model output uncertainties on the basis of model input uncertainties, accounting for the full range of variation of the variables.

A well-known and widely used GSA method is Sobol’ analysis (Sobol’, 1993), which relies on the functional ANOVA (analysis of variance) decomposition (Efron and Stein, 1981). For a square-integrable model and independent input variables, Sobol’ analysis determines which part of the model output variance can be attributed to each input and to each interaction between inputs. The overall contribution of each input, including interactions with other inputs, is provided by the total Sobol’ index (Homma and Saltelli, 1996). Sobol’ indices can be estimated efficiently using various Monte Carlo-based techniques as well as metamodel-based techniques (Prieur and Tarantola, 2017). The latter save on expensive model evaluations by first performing a small number of model runs, which are used to compute an accurate approximation to the original model – the meta- or surrogate model – from which the Sobol’ indices are finally computed (Fang et al., 2006; Le Gratiet et al., 2017).

One of the most popular and powerful metamodeling methods is the polynomial chaos expansion (PCE) (Ghanem and Spanos, 1990). PCE represents the model in a specific basis consisting of polynomials that are orthonormal with respect to the input distribution. Its strength stems from the fact that once the expansion is computed, it easily gives all the variance-based quantities defined through the ANOVA decomposition, and in particular the Sobol’ indices at all orders (Sudret, 2008). In practice, the expansion cannot use infinitely many terms and must be truncated. Among the many approaches available to compute the expansion coefficients, sparse regression techniques combined with adaptive basis selection appear to be especially promising (see Lüthen et al. (2021b,a) for an overview). Here, a small number of terms is selected which is able to best represent the computational model based on the available model evaluations.

In some practical situations, partial derivatives of the model output with respect to each input are easily accessible, for example by algorithmic differentiation of the numerical model in the reverse (adjoint) mode (Griewank and Walther, 2008). This technique allows for computing all partial derivatives of the model output at a cost independent of the number of input variables. Since PCEs are such a well established metamodeling tool, there have been many efforts to leverage the additional information contained in model derivatives to improve the performance of the PCE, however with mixed success: The idea of including derivative information into sparse regression problems, often called *gradient-enhanced ℓ^1 -minimization*, is tested by Jake-man et al. (2015) for one numerical example with uniform inputs, and analyzed theoretically and numerically by Peng et al. (2016) for Hermite PCE. Both report favorable results. Roderick et al. (2010) and Li et al. (2011) apply polynomial regression (PCE) in the context of nuclear engineering. They include derivative information into the least-squares regression formulation and observe that most polynomial families are not orthogonal with respect to the H^1 inner product, which destroys the orthogonality of the regression matrix. To alleviate this issue, Guo et al.

(2018) develop a preconditioning procedure for gradient-enhanced sparse regression with certain polynomial families, with the goal of improving the orthogonality properties of the regression matrix. Gejadzea et al. (2019) propose to use gradients for the projection-based computation of PCE coefficients. In all these approaches, the inclusion of derivative information is not straightforward, but requires specific polynomial families (in particular Hermite) or elaborate techniques like preconditioning, because the partial derivatives of a PCE basis do in general not form an orthogonal system.

On a different note, the availability of model derivatives has implications also for GSA. The so-called *Derivative-based Global Sensitivity Measures* (DGSM) are computed by integrating the squared partial derivatives of the model output over the domain of the inputs. These indices have been shown to be efficiently estimated by sampling techniques (as Monte Carlo or quasi-Monte Carlo) as well as from PCE (Sudret and Mai, 2015) and have been proven to be an excellent screening technique (i.e., for detecting all the non-influential inputs among a large number), see e.g. the review in Kucherenko and Iooss (2017). Indeed, the interpretation of DGSM indices is straightforward due to their inequality relationship with Sobol’ indices: multiplied with an optimal Poincaré constant, DGSM indices provide a narrow upper bound of the total Sobol’ index (Roustant et al., 2017), regardless of the input probability distribution.

Another way to utilize model derivatives, which solves the issues present for the polynomial chaos formulation, and naturally provides sharp lower bounds as well as upper bounds on total Sobol’ indices, is to compute *Poincaré chaos expansions* (Roustant et al., 2020), which we will abbreviate by *PoinCE* in the sequel. Similar to PCE, PoinCE is a spectral expansion in terms of an orthonormal basis whose elements are eigenfunctions of the so-called *Poincaré differential operator*. The eigenfunctions are in general non-polynomial, except for the special case of the Gaussian distribution, where they coincide with the Hermite polynomials. The key property of PoinCE is that the partial derivatives of the basis form again an orthogonal basis with respect to the input distribution. This allows to conveniently expand the derivative of the computational model in terms of partial derivatives of the basis (PoinCE-der), which yields another estimator for partial variances and Sobol’ indices. If the partial derivatives of the model have smaller variance than the model itself, the estimates based on the model derivatives might be more accurate. This makes PoinCE(-der) an efficient tool for screening (Roustant et al., 2020).

Our present contribution to the field of generalized chaos expansions and GSA is two-fold. On the theoretical side, we provide a proof that the Poincaré basis is in fact characterized uniquely as the orthonormal basis which remains an orthogonal basis (w.r.t. the same probability measure) after differentiation. Furthermore, we show how PoinCE naturally generalizes an analytical formula for DGSM originally developed for Hermite PCE (Sudret and Mai, 2015), which implies that PoinCE simultaneously and efficiently provides lower and upper bounds to all partial variances. On the computational side, we improve on Roustant et al. (2020), which introduced projection-based Poincaré chaos and demonstrated that small Sobol’ indices were approximated particularly well by the derivative expansion. In this contribution, we compute PoinCE by sparse regression, thus generalizing the powerful and cost-effective sparse PCE methodology to non-polynomial functions. We explore the performance of PoinCE as an estimator for partial variances (upper

and lower bounds) and compare it to standard PCE.

This paper is organized as follows. Section 2 revisits the mathematical foundations of PoinCE and presents several analytical results related to Sobol' indices and DGSM. Section 3 explains the sparse regression methodology adapted from PCE to PoinCE. The methodology is applied in section 4, where two example problems are investigated to demonstrate its performance for sensitivity analysis and screening. Finally, we summarize our conclusions in section 5.

2 Mathematical background

2.1 Orthonormal bases in L^2

In this section, we recall some important facts about orthonormal bases in $L^2(E, \mu)$ where E is a subset of \mathbb{R}^d and μ is a probability measure on E . We first outline the general theory in section 2.1.1. The particular cases of polynomial and Poincaré bases in several dimensions are developed in sections 2.1.2 and 2.1.3.

2.1.1 General theory

To begin with, recall that $L^2(E, \mu)$ endowed with the inner product

$$\langle f, g \rangle = \int_E f(x)g(x)\mu(dx), \quad \text{for } f, g \in L^2(E, \mu)$$

is a Hilbert space. Recall that a sequence of functions $(\Phi_\alpha)_{\alpha \geq 0}$ is an *orthonormal system* in $L^2(E, \mu)$ if it satisfies the two following assumptions:

- 1) For all $\alpha \neq \alpha'$, $\langle \Phi_\alpha, \Phi_{\alpha'} \rangle = 0$, (orthogonality)
- 2) For all α , $\langle \Phi_\alpha, \Phi_\alpha \rangle = 1$ (unit norm).

An orthonormal system in $L^2(E, \mu)$ is called *complete* if the closure of the span generated by (Φ_α) is $L^2(E, \mu)$. In this case, the system (Φ_α) is called an *Hilbertian* or *orthonormal basis* of $L^2(E, \mu)$ and for any function $f \in L^2(E, \mu)$ the following expansion holds:

$$f = \sum_{\alpha} \langle \Phi_\alpha, f \rangle \Phi_\alpha, \quad (\mu \text{ almost surely}). \quad (1)$$

As a corollary, for $f, g \in L^2(E, \mu)$, we obtain the Parseval formulas

$$\langle f, g \rangle = \sum_{\alpha} \langle \Phi_\alpha, f \rangle \langle \Phi_\alpha, g \rangle, \quad (2)$$

$$\|f\|^2 = \langle f, f \rangle = \sum_{\alpha} \langle \Phi_\alpha, f \rangle^2. \quad (3)$$

When used to represent random variables in terms of a basis of uncorrelated random variables, such an expansion is often called *chaos expansion* in the uncertainty quantification literature (Wiener, 1938; Ghanem and Spanos, 1991; Ernst et al., 2012).

An archetype example of chaos expansion is given by the so-called *Fourier expansion*. This corresponds to the case where the set $E = [0, 1]$ is endowed with the Lebesgue measure and we have for $\alpha \in \mathbb{Z}$,

$$\Phi_\alpha(x) = \cos(2\pi\alpha x) \text{ if } \alpha \leq 0, \text{ and } \Phi_\alpha(x) = \sin(2\pi\alpha x) \text{ otherwise.}$$

In this frame, any square-integrable function f may be expanded as

$$f(x) = a_0 + \sum_{\alpha > 0} (a_\alpha \cos(2\pi\alpha x) + b_\alpha \sin(2\pi\alpha x)).$$

Here,

$$a_0 = \int_0^1 f(x) dx, \quad a_\alpha = \int_0^1 f(x) \cos(2\pi\alpha x) dx, \quad b_\alpha = \int_0^1 f(x) \sin(2\pi\alpha x) dx, \quad \text{for all } \alpha \in \mathbb{Z}_*.$$

In the following we describe two particular chaos types, namely the classical *polynomial chaos* and the recently developed *Poincaré chaos*.

2.1.2 Polynomial chaos

A classical family of chaos expansions on an interval E of \mathbb{R} endowed with a probability measure is given by orthonormal polynomial bases. A well-known example is the Hermite expansion for which the set E is the whole line \mathbb{R} endowed with the standard Gaussian distribution. In this example, for $\alpha \in \mathbb{N}$, $\Phi_\alpha = H_\alpha$ is the Hermite polynomial of degree α . The first Hermite polynomials are

$$H_0(x) = 1, \quad H_1(x) = x, \quad H_2(x) = \frac{x^2 - 1}{2}, \quad H_3(x) = \frac{x^3 - 3x}{6}, \quad H_4(x) = \frac{x^4 - 6x^2 + 3}{24} \text{ for } x \in \mathbb{R}.$$

There is a revival of interest in orthonormal polynomial bases on \mathbb{R} . Indeed, this old nice topic in mathematics is actually pushed by the random matrix theory (see for example Anderson et al. (2010)). Orthonormal polynomial bases on \mathbb{R} are related to the so-called moment problem and have many surprising properties. For example, they may be constructed by using the Gram-Schmidt process, involving only tridiagonal Jacobi matrices. For properties of orthogonal polynomial systems, we refer to Szegő (1939) and Simon (2010).

When considering a product of intervals $E = E_1 \times E_2 \times \dots \times E_d$ endowed with a product probability measure $\mu = \mu_1 \otimes \dots \otimes \mu_d$ there is a canonical way to build a Hilbertian basis from a collection of marginal Hilbertian bases. Indeed, for $i = 1, \dots, d$ assume that $(\Phi_{\alpha_i}^{(i)})$ is a Hilbertian basis of $L^2(E_i, \mu_i)$. Then, setting $\alpha := (\alpha_1, \dots, \alpha_d)$ and $\Phi_\alpha := \prod_{i=1}^d \Phi_{\alpha_i}^{(i)}$ we obtain that (Φ_α) is an orthonormal basis of $L^2(E, \mu)$.

2.1.3 Poincaré chaos

The Poincaré basis is an example of orthonormal basis of $L^2(\mu)$, consisting of functions that admit weak derivatives, i.e. that belong to $H^1(\mu) = \{f \in L^2(\mu) \text{ s.t. } f' \in L^2(\mu)\}$. Recall that

$H^1(\mu)$, endowed with the norm $\|f\|_{H^1(\mu)}^2 = \|f\|^2 + \|f'\|^2$, is a Hilbert space. Like polynomial chaos, the multivariate Poincaré basis is obtained by tensorization of 1D orthonormal bases. Thus it is enough to describe the 1D case, and we now fix $d = 1$. This short summary is based on Roustant et al. (2017) in which more details can be found. We assume that:

Assumption 1. *The probability measure μ is supported on a bounded interval (a, b) and admits a probability density function of the form $\rho = e^{-V}$, where V is continuous and piecewise C^1 on $[a, b]$.*

This assumption is sufficient to guarantee the existence of a Poincaré basis. On the topological side, it implies that the Hilbert space $L^2(\mu)$ (resp. $H^1(\mu)$) is equal to $L^2(a, b)$ (resp. $H^1(a, b)$), with an equivalent norm. Indeed, μ is a bounded perturbation of the uniform measure on $[a, b]$, meaning that the pdf ρ is bounded from below and above by strictly positive constants (by continuity of V on the compact support $[a, b]$).

Theorem 1 (1D Poincaré basis). *Under Assumption 1, there exists an orthonormal basis $(\varphi_\alpha)_{\alpha \geq 0}$ of $L^2(\mu)$ such that for all $f \in H^1(\mu)$ and for all integer $\alpha \geq 0$, we have:*

$$\langle f', \varphi'_\alpha \rangle = \lambda_\alpha \langle f, \varphi_\alpha \rangle \quad (4)$$

where $(\lambda_\alpha)_{\alpha \geq 0}$ is an increasing sequence that tends to infinity:

$$0 = \lambda_0 < \lambda_1 < \lambda_2 < \dots < \lambda_\alpha \xrightarrow{\alpha \rightarrow \infty} +\infty.$$

The basis functions φ_α are unique up to a sign change, and form the so-called Poincaré basis. Notice that φ_0 is a constant function equal to ± 1 ; by convention, we choose $\varphi_0 = 1$. Furthermore, the Poincaré basis functions are the eigenfunctions of the differential operator

$$L(f) = f'' - V'f'$$

i.e. satisfy $L(f) = -\lambda f$, subject to Neumann conditions $f'(a) = f'(b) = 0$. The $(\lambda_\alpha)_{\alpha \geq 0}$ are the corresponding eigenvalues. Finally, $\alpha^{-2}\lambda_\alpha \rightarrow \pi^2$ when α tends to infinity, and for all $\alpha \in \mathbb{N}^*$, the eigenfunction φ_α has exactly $\alpha - 1$ zeros in (a, b) .

Proof. The main part of the Theorem can be found in Roustant et al. (2017) or Bakry et al. (2014). The two last assertions come by rewriting the differential equation $V'' - V'f' = -\lambda f$ in the Sturm-Liouville form

$$-(pf')' + qf = \lambda wf$$

with $p = w = \rho$ and $q = 0$. Then, by the Sturm-Liouville theory (see e.g. Zettl (2010, Theorem 4.3.1, (1), (6) and (7))), we have that $\alpha^{-2}\lambda_\alpha \rightarrow \pi^2$ when α tends to infinity, and for all $\alpha \in \mathbb{N}^*$, the eigenfunction φ_α has exactly $\alpha - 1$ zeros in (a, b) . \square

The Poincaré basis shares some similarity with both the polynomial chaos and the Fourier basis in terms of oscillations: by Theorem 1, the higher the order of the eigenvalue, the more oscillating the corresponding eigenfunction.

For some specific cases, the Poincaré basis is known analytically. For instance, for the uniform distribution, the Poincaré basis is a kind of Fourier basis (see e.g. Roustant et al. (2020), §4). Otherwise it has to be computed numerically, e.g., by a finite element technique (see section 3.1).

Note that Assumption 1 is a convenient sufficient condition which guarantees the existence of a Poincaré basis. It is satisfied for a large range of truncated probability distributions. The set of probability distributions for which the Poincaré chaos exists is larger, but not well known. For instance, the Poincaré chaos is defined for the Gaussian distribution, and then coincides with polynomial chaos, corresponding to Hermite polynomials. This is the only case where Poincaré chaos and polynomial chaos coincide (Bakry et al., 2014, §2.7). On the other hand, Poincaré chaos is not defined for the Laplace distribution, since the eigenvalues of the associated operator do not form a countable set (Bakry et al., 2014, §4.4.1).

The Poincaré basis is useful for sensitivity analysis. First, it is linked to the Poincaré inequality

$$\text{Var}_\mu(f) \leq C_P(\mu) \int f'^2 d\mu, \quad (5)$$

which holds for all functions $f \in H^1(\mu)$ under the assumptions on μ . Indeed, the smallest constant $C_P(\mu)$ such that (5) is satisfied is equal to $C_P(\mu) = 1/\lambda_1$, and choosing $f = \varphi_1$ corresponds to the equality case. Roughly speaking, the Poincaré basis function associated to the first non-zero eigenvalue gives the best “control” of the variability of f by its derivative (in the L^2 sense). A second appealing property for the analysis of variance is that the derivatives of the Poincaré basis remain orthogonal functions:

Proposition 1. *Under Assumption 1, the sequence $\left(\frac{1}{\sqrt{\lambda_\alpha}}\varphi'_\alpha\right)_{\alpha \geq 1}$ is an orthonormal basis of $L^2(\mu)$.*

Proof. The orthonormality of the sequence is a consequence of (4) by choosing $f = \varphi_\beta$, with $\beta \in \mathbb{N}^*$. It remains to show that the system is dense in $L^2(\mu)$, or equivalently, that its orthogonal is null. Let thus $f \in L^2(\mu)$ such that

$$\langle f, \varphi'_\alpha \rangle = 0, \quad \text{for all } \alpha \geq 1.$$

As explained when stating Assumption 1, $L^2(\mu)$ (resp. $H^1(\mu)$) is equal to $L^2(a, b)$ (resp. $H^1(a, b)$), with an equivalent norm. Now, there exists $g \in H^1(\mu)$ such that $f = g'$. Indeed, let us define g by $g(x) = g(a) + \int_a^x f(t)dt$. As $f \in L^2(\mu) = L^2(a, b)$, then g belongs to $H^1(a, b) = H^1(\mu)$, and $g' = f$. Then we have

$$\langle g', \varphi'_\alpha \rangle = 0, \quad \text{for all } \alpha \geq 1.$$

By (4), we obtain $\langle g, \varphi_\alpha \rangle = 0$ for all $\alpha \geq 1$ (as $\lambda_\alpha > 0$ for $\alpha \geq 1$). As the functions φ_α form an orthonormal basis of $L^2(\mu)$ with $\varphi_0 = 1$, this implies that g is a constant function, and finally $f = 0$. The proof is completed. \square

In fact, the property in Proposition 1, i.e., that the derivatives of the Poincaré basis form again an orthonormal system in $L^2(\mu)$, uniquely characterizes the Poincaré basis:

Proposition 2. *Under Assumption 1, Poincaré bases are the only orthonormal bases (φ_α) of $L^2(\mu)$ in $H^1(\mu)$ such that (φ'_α) is an orthogonal basis of $L^2(\mu)$.*

This result seems difficult to find in the literature. German-speaking readers can find a similar proposition in Mikolas (1955), stated in the frame of Sturm-Liouville theory for twice-differentiable functions satisfying boundary conditions. We provide below a proof based on Hilbertian arguments.

As a corollary, if there exists a basis different from the Poincaré basis for which derivatives form an orthogonal system, then that system is not dense in $L^2(\mu)$. As an example, for the uniform probability measure on $[0, 2\pi]$, consider the usual Fourier basis formed by $\{\cos(nx), \sin(nx) : n \geq 0\}$ (up to multiplicative constants). Taking derivatives results in the same set of functions (up to multiplicative constants) – except for the constant function $\cos(0x) = 1$. Thus, the derivatives form an orthogonal system which covers the orthogonal of constant functions in $L^2(\mu)$, which is a strict subspace of $L^2(\mu)$. Meanwhile, the Poincaré basis for this probability measure is formed by functions proportional to $\cos(\frac{n}{2}x)$ for $n \geq 0$. Proposition 2 guarantees that all functions of $L^2(\mu)$, including the constant functions, are spanned by the derivatives, which is explained intuitively by the presence of half-frequencies: when n is odd, the functions $\cos(\frac{n}{2}x)$ are not orthogonal to 1.

Proof of Proposition 2. The fact that a Poincaré basis remains an orthogonal basis by derivation has been proved in Proposition 1. Conversely, let $(\varphi_\alpha)_{\alpha \geq 0}$ be a system of $H^1(\mu)$, with $\varphi_0 = 1$, such that (φ_α) is an orthonormal basis of $L^2(\mu)$ and $(\varphi'_\alpha)_{\alpha \geq 1}$ is an orthogonal basis of $L^2(\mu)$. Let us first prove that (φ_α) is an orthogonal basis of $H^1(\mu)$. The orthogonality is a direct consequence of the definition of the norm of $H^1(\mu)$:

$$\langle \varphi_\alpha, \varphi_\beta \rangle_{H^1(\mu)} = \langle \varphi_\alpha, \varphi_\beta \rangle_{L^2(\mu)} + \langle \varphi'_\alpha, \varphi'_\beta \rangle_{L^2(\mu)} = (1 + \|\varphi'_\alpha\|_{L^2(\mu)}^2) \delta_{\alpha,\beta}.$$

Let us prove that (φ_α) is dense in $H^1(\mu)$. As explained when stating Assumption 1, $L^2(\mu)$ (resp. $H^1(\mu)$) is equal to $L^2(a, b)$ (resp. $H^1(a, b)$), with an equivalent norm. Hence, it is equivalent to prove that (φ_α) is dense in $H^1(a, b)$. Now let f be in $H^1(a, b)$. As (φ'_α) is dense in $L^2(a, b)$ (equivalently in $L^2(\mu)$), then f' is written $f' = \sum_{\alpha \in \mathbb{N}} c_\alpha \varphi'_\alpha$. In $H^1(a, b)$ each function is equal to the primitive of its derivative, hence we have:

$$\begin{aligned} \left| f(t) - f(a) - \sum_{\alpha=1}^N c_\alpha (\varphi_\alpha(t) - \varphi_\alpha(a)) \right| &= \left| \int_a^t \left(f'(x) - \sum_{\alpha=1}^N c_\alpha \varphi'_\alpha(x) \right) dx \right| \\ &\leq (b-a) \left\| f' - \sum_{\alpha=1}^N c_\alpha \varphi'_\alpha \right\|_{L^2(a,b)} \end{aligned}$$

where the inequality comes from the Cauchy-Schwarz inequality. We deduce that $\|f - f(a) - \sum_{\alpha=1}^N c_\alpha (\varphi_\alpha - \varphi_\alpha(a))\|_{L^2(a,b)} \rightarrow 0$ when N tends to infinity. Together with $f' = \sum_{\alpha \in \mathbb{N}} c_\alpha \varphi'_\alpha$, this implies that $\|f - f(a) - \sum_{\alpha=1}^N c_\alpha (\varphi_\alpha - \varphi_\alpha(a))\|_{H^1(a,b)} \rightarrow 0$. As $\varphi_0 = 1$, this proves that (φ_α) is dense in $H^1(a, b)$, which was to prove.

Now, let us fix $\alpha \geq 0$. Consider the linear form L_α defined on $H^1(\mu)$ by $L_\alpha(f) = \langle f', \varphi'_\alpha \rangle_{L^2(\mu)}$.

By the Cauchy-Schwarz inequality, we have $|L_\alpha(f)| \leq \|f'\|_{L^2(\mu)} \|\varphi'_\alpha\|_{L^2(\mu)} \leq \|f\|_{H^1(\mu)} \|\varphi'_\alpha\|_{L^2(\mu)}$, which proves that L_α is continuous. Hence, by the Riesz representation theorem, there exists a unique $\zeta_\alpha \in H^1(\mu)$ such that for all $f \in H^1(\mu)$, $L_\alpha(f) = \langle f, \zeta_\alpha \rangle_{H^1(\mu)}$, i.e. $\langle f', \varphi'_\alpha \rangle_{L^2(\mu)} = \langle f, \zeta_\alpha \rangle_{H^1(\mu)}$. Choosing $f = \varphi_\beta$ with $\beta \neq \alpha$, we obtain by orthogonality of (φ'_α) , that for all $\beta \neq \alpha$, $\langle \varphi_\beta, \zeta_\alpha \rangle_{H^1(\mu)} = 0$. As $(\varphi_\beta)_{\beta \geq 0}$ is an orthogonal basis of $H^1(\mu)$, this implies that ζ_α is collinear to φ_α : there exists $\tilde{\lambda}_\alpha \in \mathbb{R}$ such that $\zeta_\alpha = \tilde{\lambda}_\alpha \varphi_\alpha$. Thus, for all $f \in H^1(\mu)$, we have $\langle f', \varphi'_\alpha \rangle_{L^2(\mu)} = \tilde{\lambda}_\alpha \langle f, \varphi_\alpha \rangle_{H^1(\mu)}$. Choosing $f = \varphi_\alpha$, we get $\tilde{\lambda}_\alpha = \frac{\|\varphi'_\alpha\|_{L^2(\mu)}^2}{1 + \|\varphi'_\alpha\|_{L^2(\mu)}^2}$, which belongs to $[0, 1)$. Finally, we obtain that $\langle f', \varphi'_\alpha \rangle_{L^2(\mu)} = \lambda_\alpha \langle f, \varphi_\alpha \rangle_{L^2(\mu)}$, where $\lambda_\alpha = \frac{\tilde{\lambda}_\alpha}{1 - \tilde{\lambda}_\alpha}$ is a non-negative real number. As it is true for all f in $H^1(\mu)$ and all $\alpha \in \mathbb{N}$, this implies, by uniqueness of the Poincaré basis (under Assumption 1), that $(\varphi_\alpha)_{\alpha \geq 0}$ is a Poincaré basis. \square

In higher dimensions, we assume that for all $i = 1, \dots, d$, the probability measure μ_i satisfies Assumption 1, and we denote by $(\varphi_{i,\alpha_i})_{\alpha_i \geq 0}$ the sequence of 1-dimensional Poincaré basis functions, and by $(\lambda_{i,\alpha_i})_{\alpha_i \geq 0}$ the sequence of associated eigenvalues. The Poincaré chaos basis is then defined by the tensor product $\Phi_\alpha = \varphi_{1,\alpha_1} \otimes \dots \otimes \varphi_{d,\alpha_d}$. Using the properties of L^2 bases, (4) thus implies that for all $f \in H^1(\mu)$, for all $i = 1, \dots, d$:

$$\left\langle \frac{\partial f}{\partial x_i}, \frac{\partial \Phi_\alpha}{\partial x_i} \right\rangle = \lambda_{i,\alpha_i} \langle f, \Phi_\alpha \rangle. \quad (6)$$

Similarly, applying Prop. 1, we have:

Proposition 3. *Under Assumption 1, for all $i = 1, \dots, d$, the sequence $\left(\frac{1}{\sqrt{\lambda_{i,\alpha_i}}} \frac{\partial \Phi_\alpha}{\partial x_i} \right)_{\alpha, \alpha_i \geq 1}$ is an orthonormal basis of $L^2(\mu)$.*

2.2 Variance-based indices, derivative-based indices

We first recall the definition of variance-based sensitivity indices, which allow us to explain the variability of a function output by its input variables with a variance decomposition formula.

Let f be a real-valued function defined on $E = E_1 \times \dots \times E_d \subseteq \mathbb{R}^d$. The uncertainty of the inputs is represented by a random vector $\mathbf{X} = (X_1, \dots, X_d)^T$ with probability measure μ on E . We further assume that the X_i 's are independent and that $f(\mathbf{X})$ belongs to $L^2(E, \mu)$. Denoting by μ_i the marginal distribution of X_i on E_i ($i = 1, \dots, d$), we then have $\mu = \mu_1 \otimes \dots \otimes \mu_d$. In this framework, $f(\mathbf{X})$ can be decomposed uniquely as a sum of terms of increasing complexity

$$f(\mathbf{X}) = f_0 + \sum_{1 \leq i \leq d} f_i(X_i) + \sum_{1 \leq i < j \leq d} f_{i,j}(X_i, X_j) + \dots + f_{1,\dots,d}(X_1, \dots, X_d) \quad (7)$$

under centering conditions $\mathbb{E}[f_I(X_I)] = 0$ and non-overlapping conditions $\mathbb{E}[f_I(X_I)|X_J] = 0$, for all sets $I \subseteq \{1, \dots, d\}$ and all strict subsets J of I . We have used the set notation X_I to represent the subvector of \mathbf{X} obtained by selecting the coordinates belonging to I . These conditions imply that all the terms of (7) are orthogonal, which leads to the variance decomposition

$$\text{Var}f(\mathbf{X}) = \sum_{1 \leq i \leq d} \text{Var}f_i(X_i) + \sum_{1 \leq i < j \leq d} \text{Var}f_{i,j}(X_i, X_j) + \dots + \text{Var}f_{1,\dots,d}(X_1, \dots, X_d) \quad (8)$$

Due to this property, the functional decomposition (7) is often called ANOVA (ANalysis Of VAriance) decomposition. Originating from Hoeffding (1948), it was revisited by Efron and Stein (1981) and Sobol' (1993). For a given set $I \subseteq \{1, \dots, d\}$, we call the corresponding term of (8) partial variance (denoted D_I), and call its normalized version Sobol' index (denoted S_I):

$$D_I = \text{Var}(f_I(X_I)), \quad S_I = \frac{D_I}{D},$$

where $D = \text{Var}f(\mathbf{X})$ is the overall variance. In particular, for $i \in \{1, \dots, d\}$, the first-order Sobol' index S_i corresponds to the proportion of variance of $f(\mathbf{X})$ explained by X_i only. In order to include also the interactions of X_i with the other variables, the total partial variance and the total Sobol' index are defined by

$$D_i^{\text{tot}} = \sum_{I \ni \{i\}} \text{Var}(f_I(X_I)), \quad S_i^{\text{tot}} = \frac{D_i^{\text{tot}}}{D}.$$

Note that practitioners also call the (total) partial variances unnormalized (total) Sobol' indices. In the sequel, we will use these two words interchangeably.

The total Sobol' index can be used for screening. Indeed, under mild conditions, $S_i^{\text{tot}} = 0$ implies that the function f does not depend on x_i over E (in the pointwise sense).

When the derivatives are available, a global sensitivity index can be obtained by integration. The so-called derivative-based sensitivity measure (DGSM) index of f with respect to X_i is defined by (see e.g. Sobol and Gresham (1995)):

$$\nu_i = \mathbb{E} \left[\left(\frac{\partial f}{\partial x_i}(\mathbf{X}) \right)^2 \right] = \int_{\mathbb{R}^d} \left(\frac{\partial f}{\partial x_i}(\mathbf{x}) \right)^2 d\mu(\mathbf{x}) = \left\| \frac{\partial f}{\partial x_i} \right\|^2. \quad (9)$$

Contrarily to variance-based indices, DGSM are not associated to a variance decomposition. Nevertheless, they can be used for screening. Indeed, under mild conditions, $\nu_i = 0$ implies that f does not depend on x_i over E .

2.3 Chaos expansion serving sensitivity analysis

One main advantage of using an orthonormal basis for sensitivity analysis is that, once the expansion has been obtained, the variance-based indices can be computed in a straightforward way as a sum of squared coefficients (Sudret, 2006, 2008). More precisely, let f be in $L^2(\mu)$, and let $(\Phi_\alpha)_{\alpha \in \mathbb{N}^d}$ be a multivariate orthonormal basis obtained by tensorization as described in section 2.1. The decomposition of f in terms of the basis is given by

$$f = \sum_{\alpha \in \mathbb{N}^d} c_\alpha \Phi_\alpha. \quad (10)$$

Then, by using the orthonormality we immediately have the expression of the total variance

$$D = \sum_{\alpha \neq \mathbf{0}} c_\alpha^2. \quad (11)$$

The expression of the total Sobol' index S_i^{tot} is obtained by only considering the terms of the decomposition (10) that contain the variable x_i , i.e. such that $\alpha_i \geq 1$. Hence, we have $S_i^{\text{tot}} = \frac{D_i^{\text{tot}}}{D}$ with D_i^{tot} the total partial variance

$$D_i^{\text{tot}} = \sum_{\alpha, \alpha_i \geq 1} c_\alpha^2. \quad (12)$$

The first-order Sobol' index S_i^1 relies on the terms that include x_i only, i.e., $S_i^1 = \frac{D_i^1}{D}$ with

$$D_i^1 = \sum_{\substack{\alpha, \alpha_i \geq 1, \\ \alpha_j = 0 \text{ for } j \neq i}} c_\alpha^2. \quad (13)$$

Let us now consider the case where the gradient of f is available. The Poincaré basis is particularly suited to this situation. Indeed, we can derive in a straightforward way expressions of both variance-based and derivative-based indices, involving the derivatives of f . Due to orthonormality, the coefficients of the basis expansion in (10) are given by the projection of f onto the associated basis element:

$$c_\alpha = \langle f, \Phi_\alpha \rangle. \quad (14)$$

From now on, let $(\Phi_\alpha)_\alpha$ denote the Poincaré basis. Combining (6) and (14), and assuming that $\alpha_1 \geq 1$, c_α can be written using 1st partial derivatives (Roustant et al., 2020):

$$c_\alpha = \langle f, \Phi_\alpha \rangle = \frac{1}{\lambda_{1,\alpha_1}} \left\langle \frac{\partial f}{\partial x_1}, \frac{\partial \Phi_\alpha}{\partial x_1} \right\rangle = \frac{1}{\lambda_{1,\alpha_1}} \left\langle \frac{\partial f}{\partial x_1}, \frac{\partial \varphi_{1,\alpha_1}}{\partial x_1} \otimes \varphi_{2,\alpha_2} \otimes \cdots \otimes \varphi_{d,\alpha_d} \right\rangle \quad (15)$$

and equivalently using i th partial derivatives if $\alpha_i \geq 1$. Thus, (11), (12) and (13) can also be computed using the i th partial derivatives of f . Whereas the theoretical expressions are equal, their estimators have different properties. For example, if the integral is evaluated by Monte Carlo simulation, the expression whose integrand has smaller variance will be more accurate. We describe in section 3 how we compute the expansions coefficients by regression in this work, and empirically compare the two estimators in section 4.

Furthermore, DGSM can be computed directly from the Poincaré expansion. More precisely, we have the following new proposition.

Proposition 4 (DGSM formula for Poincaré chaos). *Let $f \in H^1(\mu)$. Let $f = \sum_\alpha c_\alpha \Phi_\alpha$ be the expansion of f in the Poincaré chaos basis, with $c_\alpha = \langle f, \Phi_\alpha \rangle$. Then the DGSM index of f with respect to X_i is equal to:*

$$\nu_i = \sum_{\alpha, \alpha_i \geq 1} \lambda_{i,\alpha_i} (c_\alpha)^2. \quad (16)$$

Proof. Write $f = \sum_\alpha c_\alpha \Phi_\alpha$. Then by Prop. 3, we have:

$$\frac{\partial f}{\partial x_i} = \sum_{\alpha, \alpha_i \geq 1} c_\alpha \frac{\partial \Phi_\alpha}{\partial x_i},$$

where we can constrain the sum to multi-indices α such that $\alpha_i \geq 1$, since $\varphi_{i,\alpha_i} = 1$ for $\alpha_i = 0$. Now, using again the orthogonality of Poincaré basis derivatives (Prop. 3), it holds:

$$\nu_i = \left\| \frac{\partial f}{\partial x_i} \right\|^2 = \sum_{\alpha, \alpha_i \geq 1} (c_\alpha)^2 \left\| \frac{\partial \Phi_\alpha}{\partial x_i} \right\|^2 = \sum_{\alpha, \alpha_i \geq 1} \lambda_{i,\alpha_i} (c_\alpha)^2.$$

□

Formula (16) extends a previous result given by Sudret and Mai (2015) when all the μ_i are standard Gaussian. Indeed, in that case, we know that Poincaré chaos coincides with polynomial chaos. Hence, the basis functions φ_{i,α_i} are Hermite polynomials, and $\lambda_{i,\alpha_i} = \alpha_i$. Then (16) coincides with formula (51), p. 245 in Sudret and Mai (2015), with the following change of notations: $\underline{\alpha} \leftarrow \alpha, a_{\underline{\alpha}} \leftarrow c_{\alpha}, \mathcal{A}^{(i)} \leftarrow \{\alpha, \alpha_1 \geq 1\}$. Note that for general polynomial chaos expansions there exists no such simple formula for DGSM, except for a few probability distributions for which the derivatives of the polynomial basis functions can be expressed analytically in terms of the basis itself (Sudret and Mai, 2015).

Using the expressions provided in (12) and (16), we obtain lower and upper bounds to partial variances as follows. Since in practice, the sum in (12) uses only a finite subset $\mathcal{A} \subset \mathbb{N}^d$ of coefficients c_{α} , it always provides a lower bound on the total partial variance D_i^{tot} . In addition to this lower bound, the Poincaré basis provides an upper bound, relying on the DGSM computed with the derivatives of f (see Lamboni et al. (2013)):

$$\sum_{\alpha \in \mathcal{A}, \alpha_i \geq 1} (c_{\alpha})^2 \leq D_i^{\text{tot}} \leq C_P(\mu_i) \nu_i = \sum_{\alpha \in \mathbb{N}^d, \alpha_i \geq 1} \frac{\lambda_{i,\alpha_i}}{\lambda_{i,1}} (c_{\alpha})^2. \quad (17)$$

Note that these inequalities are valid for the analytical expressions, but not necessarily for their estimated values which are obtained in the next section.

3 Computation of sparse Poincaré expansions

Let $f \in H^1(\mu, E)$ be a computational model defined on the input space $E \subset \mathbb{R}^d$, with the input probability measure μ admitting a probability density function ρ fulfilling Assumption 1. In the remainder of this paper, we assume that ρ is known. We also assume that we are provided with an experimental design consisting of points $\mathcal{X} \subset E$ sampled i.i.d from the input distribution, the corresponding model evaluations $\{f(\mathbf{x}) : \mathbf{x} \in \mathcal{X}\}$, and the full gradient evaluation $\{\frac{\partial f}{\partial x_i}(\mathbf{x}) : \mathbf{x} \in \mathcal{X}, i = 1, \dots, d\}$.

With *Poincaré expansion* (PoinCE) we denote the expansion of the computational model onto the Poincaré basis

$$f(\mathbf{x}) = \sum_{\alpha} c_{\alpha} \Phi_{\alpha}(\mathbf{x}), \quad (18)$$

and with *Poincaré derivative expansion in direction i* (PoinCE-der- i) the expression

$$\frac{\partial f}{\partial x_i}(\mathbf{x}) = \sum_{\alpha, \alpha_i \geq 1} c_{\alpha}^{\partial, i} \frac{\partial \Phi_{\alpha}}{\partial x_i}(\mathbf{x}), \quad (19)$$

or the equivalent expansion using normalized basis derivatives that have unit norm in $L^2(\mu)$. Note that (19) is the i th partial derivative of (18). Because the zeroth order basis function in a Poincaré basis is the constant function, basis terms for which $\alpha_i = 0$ have zero i th partial derivative and are not included in (19). While in theory by Equation (15), the two expressions (18) and (19) provide identical coefficients for corresponding basis elements, i.e., $c_{\alpha} = c_{\alpha}^{\partial, i}$ for $\alpha \in \{\alpha' \in \mathcal{A} : \alpha'_i \geq 1\}$, in practice they will not coincide when estimated from a data set of finite size. This will be investigated in section 4 for a number of numerical examples.

In this section, we describe how such expansions are computed in practice: this concerns the computation of the Poincaré basis functions, the choice of truncation, the location of the sampled points, and the method for computing the coefficients. The implementation relies on and integrates into the UQLab framework (Marelli and Sudret, 2014).

3.1 Implementation of Poincaré basis functions

As described in section 2.1.3, Poincaré basis functions are tensor products of univariate Poincaré basis functions. Each 1D basis consists of the eigenfunctions of the Poincaré differential operator associated with the respective marginal distribution (Theorem 1).

A Poincaré basis is guaranteed to exist for marginal distributions fulfilling Assumption 1 and for the Gaussian distribution. Other distributions have to be transformed or truncated to allow for a Poincaré basis. Since an isoprobabilistic transformation to standard variables can be highly nonlinear (Torre et al., 2019; Oladyshkin and Nowak, 2012), we opt for truncation: if the distribution is not Gaussian and has (one- or two-sided) unbounded support, we truncate it to its 10^{-6} - and $(1 - 10^{-6})$ -quantiles, respectively.¹

We consider here only standard parametric families of probability densities (bounded and unbounded), although a Poincaré basis can be computed for any input distribution which after truncation fulfills Assumption 1. In particular, without any changes to the methodology PoinCE could be used in a data-driven framework (Torre et al., 2019) by computing the Poincaré basis for a dimensionwise kernel density estimate of the input distribution (assuming independence) given the available data.

As can be seen from applying the change-of-variables formula for a linear transformation to (4), the eigenvalues of the Poincaré differential operator scale with the inverse of the squared support interval length. To avoid numerical difficulties, we therefore linearly transform (i.e., shift and rescale) parametric families to standard parameters using

- their bounds in the case of uniform, beta, triangular;
- their location and scale parameter in the case of Gaussian, Gumbel, Gumbel-min, Laplace, logistic;
- their (inverse) scale parameter in the case of exponential, gamma, Weibull, lognormal.

In the current implementation, distributions not belonging to this group of families are not being rescaled.

For standard uniform ($\mathcal{U}([-1, 1])$) and standard Gaussian ($\mathcal{N}(0, 1)$) marginals, the Poincaré basis can be analytically computed and is given by the Fourier (cosine) basis and the Hermite poly-

¹One might argue that this can distort the results obtained with PoinCE, especially in the tails. It is true that this truncation introduces a small error. However, as all such methods, PoinCE by design approximates accurately mainly the bulk, not the tails (for this, specialized techniques like subset simulation shall be used). Furthermore, in practical applications it is a modelling choice how to represent the input distribution. Choosing an unbounded parametric distribution is common, but not necessarily the most sensible choice, since for virtually every quantity in the real world there is an upper bound that cannot be exceeded.

nomial basis, respectively (Roustant et al., 2020). Therefore, in the special case of uniform or Gaussian marginals, we always (after rescaling) use the analytical solution.

For all other marginals, the Poincaré basis is computed numerically using linear finite elements. We use a fine uniform grid within the bounds and piecewise linear functions with local support, commonly called ‘hat’ functions. Using the weak formulation of the eigenvalue problem of the Poincaré differential operator given in (4), we arrive at the shifted generalized eigenvalue problem

$$\mathbf{K}\mathbf{a}^{(n)} = (\lambda_n + 1)\mathbf{M}\mathbf{a}^{(n)} \quad (20)$$

as described in Roustant et al. (2017, section 4.3), where the eigenvector $\mathbf{a}^{(n)}$ denotes the vector of coefficients used to express eigenfunction φ_n in terms of ‘hat’ functions. Here \mathbf{M} is the mass matrix, whereas \mathbf{K} is the sum of mass- and stiffness matrix. After solving this problem using Matlab’s builtin function `eigs`, we interpolate the discrete eigenvectors with piecewise cubic splines,² prescribing zero derivatives at the interval boundaries. Then, the basis derivatives are computed using centered finite differences. While more sophisticated techniques (in particular, Hermitian C^1 elements) could of course be used to improve this numerical computation procedure, it is accurate enough for our purposes of demonstrating the usefulness of PoinCE (see also Appendix A). Eigenfunctions and eigenfunction derivatives are scaled to have unit norm with respect to the measure μ_i . Note that by (4), unnormalized eigenfunction derivatives have norm $\|\varphi'_{i,\alpha_i}\|_\mu = \sqrt{\lambda_{i,\alpha_i}}$ (see also Proposition 1).

3.2 Choice of the basis truncation

In practice, the series in (18) and (19) cannot include an infinite number of terms, but must be truncated to a finite expansion. We denote by $\mathcal{A} \subset \mathbb{N}^d$ the subset of multi-indices that are included in the expansion. In PCE, \mathcal{A} is typically chosen to include terms up to a certain degree p , resulting in the so-called *total degree basis*

$$\mathcal{A}^p = \{\boldsymbol{\alpha} \in \mathbb{N}^d : \sum_{i=1}^d |\alpha_i| \leq p\}. \quad (21)$$

Another common truncation method is *hyperbolic truncation* (Blatman and Sudret, 2011)

$$\mathcal{A}^{p,q} = \{\boldsymbol{\alpha} \in \mathbb{N}^d : \|\boldsymbol{\alpha}\|_q \leq p\}. \quad (22)$$

with the ℓ^q -(quasi-)norm $\|\boldsymbol{\alpha}\|_q = \left(\sum_{i=1}^d \alpha_i^q\right)^{\frac{1}{q}}$ for $q \in (0, 1]$. Since the Poincaré basis is in general not polynomial, the concept of polynomial degree cannot be used to characterize the basis functions. Instead, we use the natural order of the basis functions corresponding to the increasing sequence of Poincaré eigenvalues, which also corresponds to an increasing number of oscillations (Theorem 1; recall that the n th eigenfunction has $n - 1$ zeros). Therefore, we use

²Note on regularity: Cubic splines are of class C^2 . The eigenfunctions are at least of class C^1 , and of class C^{k+1} if the corresponding pdf is of class C^k (Roustant et al., 2017, Theorem 2). It holds $k \geq 2$ for all parametric distributions mentioned earlier except for the triangular distribution, which is only of class C^1 in $x = 0$ (see Appendix A).

the PCE terminology “degree” also for PoinCE. In particular, a degree of $\alpha_i = 0$ denotes the constant basis function $\varphi_{i,0}(x_i) = 1$ associated to the eigenvalue $\lambda_{i,0} = 0$.

Often, in practice it is not known which degree is needed for a given problem. While in theory the expansion is more accurate the larger the total degree is, in practice accuracy is limited by the number of available sample points, since the quality of the regression solution (see section 3.3) depends on the ratio of sample points to basis elements. In that case, a successful strategy consists of applying *degree adaptivity* (Blatman and Sudret, 2011; Lüthen et al., 2021a): several expansions are computed for an increasing total degree. Then, an estimate of the error of each expansion is computed, and the expansion with the smallest error estimate is chosen as the final one. This procedure is computationally inexpensive, since it only requires a new surrogate model fit for each new total degree, but no additional model evaluations. We use as error estimator the *leave-one-out (LOO) cross-validation* error (Blatman and Sudret, 2011), which is an estimator for the global $L^2(\mu)$ -error. To avoid overfitting, we use the *modified LOO* with a modification factor introduced by Chapelle et al. (2002) (see also Blatman and Sudret (2011)).

Denote by $P = |\mathcal{A}|$ the number of basis elements in the truncated expansion. \mathcal{A} , also called *candidate basis*, contains the basis elements available for approximation. We describe below how sparse regression selects a subset of \mathcal{A} to be *active*, i.e., have a nonzero coefficient. The final expansion might (and indeed often will) have less than P active terms.

3.3 Computation of the coefficients by sparse regression

For computing the coefficients of an orthogonal expansion as in (18) and (19), there exist two main approaches. One is *projection*: the model f is projected onto the basis functions, see (1). The resulting integral may be evaluated by Monte Carlo (MC) simulation, as done by Roustant et al. (2020) for Poincaré chaos, or by (sparse) quadrature methods (Gerstner and Griebel, 1998; Keese and Matthies, 2003; Knio and Le Maitre, 2006). However, note that in general MC converges slowly, while quadrature is heavily affected by the curse of dimensionality.

The second approach is *regression*, introduced for PCE by Blatman and Sudret (2008). Here, after choosing an *experimental design* $\mathcal{X} = \{\mathbf{x}^{(1)}, \dots, \mathbf{x}^{(N)}\}$ of input points, (18) is discretized as

$$\mathbf{y} \approx \mathbf{\Psi} \mathbf{c} \quad (23)$$

where $\mathbf{y} = (f(\mathbf{x}^{(1)}), \dots, f(\mathbf{x}^{(N)}))^T$ is the vector of model evaluations, $\mathbf{\Psi} \in \mathbb{R}^{N \times P}$ is the regression matrix with entries

$$\Psi_{kj} = \Phi_j(\mathbf{x}^{(k)}) \quad (24)$$

where j refers to an enumeration of the multivariate basis $(\Phi_\alpha)_{\alpha \in \mathcal{A}}$, and \mathbf{c} is the vector of expansion coefficients. The discretization of (19) is analogous, with a vector

$$\mathbf{y}_{\partial,i} = \left(\frac{\partial f}{\partial x_i}(\mathbf{x}^{(1)}), \dots, \frac{\partial f}{\partial x_i}(\mathbf{x}^{(N)}) \right)^T \quad (25)$$

containing model partial derivatives and a regression matrix $\Psi_{\partial,i}$ with entries

$$\Psi_{kj}^{\partial,i} = \frac{1}{\sqrt{\lambda_{i,\alpha_j(i)}}} \frac{\partial \Phi_j}{\partial x_i}(\mathbf{x}^{(k)}), \quad (26)$$

where $\alpha_j(i)$ denotes the i th component of the j th basis element characterized by the multi-index α_j (see also Proposition 3).

The regression problem can be solved by ordinary least squares as

$$\hat{\mathbf{c}} = \arg \min_{\mathbf{c}} \|\Psi \mathbf{c} - \mathbf{y}\|_2^2, \quad (27)$$

provided that enough model evaluations are available – at least $N \geq P$, or better $N \geq kP$ with $k = 2, 3$ to avoid overfitting. Due to the rapid growth of the total-degree basis with increasing dimension and degree, this requirement on model evaluations is often too restrictive for real-world problems.

To avoid this problem, sparse regression can be used, which regularizes the problem by encouraging solutions with few nonzero coefficients. An example is ℓ^1 -minimization:

$$\hat{\mathbf{c}} = \arg \min_{\mathbf{c}} \|\Psi \mathbf{c} - \mathbf{y}\|_2^2 + \lambda \|\mathbf{c}\|_1. \quad (28)$$

The ℓ^1 -norm penalizes the coefficient vector so that sparse solutions are preferred. The sparse regression formulation allows for accurate solutions even in the case $N < P$. There exist many sparse regression methods utilizing different formulations of the sparse regression problem, see e.g. Lüthen et al. (2021b) for an overview of available sparse regression solvers in the context of PCE. In this work, we use the sparse solver Hybrid Least Angle Regression (Hybrid-LARS) (Blatman and Sudret, 2011; Marelli et al., 2021).

A result by Candès and Plan (2011) on sparse recovery emphasizes the importance of *isotropy* of the row distribution of the regression matrix, i.e., the requirement that for a row $\mathbf{a} = (\Phi_{\alpha_1}(\mathbf{x}), \dots, \Phi_{\alpha_P}(\mathbf{x}))$ of the regression matrix Ψ it holds that $\mathbb{E}[\mathbf{a}^T \mathbf{a}] = I_P$, where I_P is the identity matrix of size P , and the expectation is with respect to the distribution of the experimental design points. If the experimental design points are chosen to follow the input distribution, the distributions of regression matrix rows for Poincaré as well as for normalized Poincaré derivative expansions are isotropic by construction due to orthonormality of the bases w.r.t. the input distribution. To improve the space-filling property of the experimental design, we use Latin Hypercube Sampling (LHS) (McKay et al., 1979) with maximin distance optimization.

3.4 Coefficients and Sobol’ indices for Poincaré derivative expansions

Due to the rescaling of the input distribution described in section 3.1, and the normalization of the PoinCE-der- i basis elements to unit norm, the computed regression coefficients first have to be rescaled with the appropriate factors before they can be postprocessed to partial variances: if the vector $\hat{\mathbf{c}}^{\partial,i}$ is the regression solution using normalized (see Proposition 1) and rescaled

(see section 3.1) basis partial derivatives, then the regression solution to (19) is the vector $\tilde{\mathbf{c}}^{\partial,i}$ with entries

$$\tilde{c}_{\boldsymbol{\alpha}}^{\partial,i} = \frac{\gamma_i}{\sqrt{\lambda_{i,\alpha_i}}} \hat{c}_{\boldsymbol{\alpha}}^{\partial,i} \quad \text{for } \boldsymbol{\alpha} \in \{\boldsymbol{\alpha}' \in \mathcal{A} : \alpha'_i \geq 1\} \quad (29)$$

where γ_i is the factor by which the i th input was divided in order to get to standard parameters. Theoretically, $\tilde{c}_{\boldsymbol{\alpha}}^{\partial,i}$ is equal to the PoinCE solution $c_{\boldsymbol{\alpha}}$ from (18), however when estimated from a data set of finite size they will in general not coincide.

By construction, the i th Poincaré derivative expansion (PoinCE-der- i , (19)) only provides coefficients corresponding to the basis elements from the set $\{\boldsymbol{\alpha} \in \mathcal{A} : \alpha_i \geq 1\}$, since the i th partial derivatives of the basis elements $\{\boldsymbol{\alpha} \in \mathcal{A} : \alpha_i = 0\}$ are zero and therefore no coefficient value can be computed for those elements. The set $\{\boldsymbol{\alpha} \in \mathcal{A} : \alpha_i \geq 1\}$ is sufficient for computing partial variances for variable i as in (12) and (13), but not enough for computing the total variance (11), which requires all coefficients $c_{\boldsymbol{\alpha}}, \boldsymbol{\alpha} \in \mathcal{A}$, and which is needed for normalizing the partial variances to Sobol' indices. To compute the total variance from PoinCE-der expansions, we therefore propose to aggregate the coefficients of all d PoinCE-der- i expansions into one vector $\tilde{\mathbf{c}}^{\partial,\text{avg}}$ as follows:

$$\tilde{c}_{\boldsymbol{\alpha}}^{\partial,\text{avg}} = \frac{1}{\#\{i : \alpha_i \geq 1\}} \sum_{i:\alpha_i \geq 1} \tilde{c}_{\boldsymbol{\alpha}}^{\partial,i} \quad \text{for each } \boldsymbol{\alpha} \in \mathcal{A} \setminus \mathbf{0}, \quad (30)$$

i.e., every PoinCE-der- i expansion which computed a coefficient value for the basis element with index $\boldsymbol{\alpha}$ contributes equally to the averaged value. It follows that in theory, the averaged coefficient $\tilde{c}_{\boldsymbol{\alpha}}^{\partial,\text{avg}}$ is equal to the PoinCE solution $c_{\boldsymbol{\alpha}}$ from (18), too. It can therefore be used to estimate the total variance according to (11).

Let $\tilde{\mathbf{c}}_{\boldsymbol{\alpha}}^{\partial,\text{avg}} = (c_{\boldsymbol{\alpha}}^{\partial,\text{avg}})_{\boldsymbol{\alpha} \in \mathcal{A} \setminus \mathbf{0}}$ be in the form of a column vector in $\mathbb{R}^{(P-1) \times 1}$. In order to use the averaged PoinCE-der expansion also as a surrogate model, we estimate the remaining coefficient $c_{\mathbf{0}}^{\partial,\text{avg}}$ corresponding to the constant term by ordinary least-squares on the residual \mathbf{y}_{res} :

$$\mathbf{y}_{\text{res}} = \mathbf{y} - \Psi \begin{pmatrix} 0 \\ \tilde{\mathbf{c}}_{\boldsymbol{\alpha}}^{\partial,\text{avg}} \end{pmatrix}, \quad (31)$$

$$c_{\mathbf{0}}^{\partial,\text{avg}} = \frac{1}{N} \sum_{k=1}^N \mathbf{y}_{\text{res}}^{(k)} \quad (32)$$

4 Numerical results

We investigate the performance of PoinCE (both based on model evaluations and on derivatives) on two numerical examples. The focus of our study is on Sobol' sensitivity analysis, but we also investigate DGSM-based upper bounds to partial variances, validation error (relative mean-squared error) and sparsity. Our implementation is based on UQLab (Marelli and Sudret, 2014) and integrates into its PCE module (Marelli et al., 2021).

We use the following estimation techniques to compute the Sobol' indices of the models:

- PCE-LARS: PCE computed by LARS (with generalized polynomial chaos adapted to the respective input) (Blatman and Sudret, 2011)

- PoinCE-MC / PoinCE-der-MC: MC-based computation using the Poincaré basis/the Poincaré partial derivative basis as in Roustant et al. (2020)
- PoinCE-LARS / PoinCE-der-LARS: Poincaré expansion and Poincaré derivative expansion computed by LARS (see section 3.3)

Partial variances are normalized to Sobol' indices using the total variance. For PCE-LARS and PoinCE-LARS, the total variance is computed from the expansion coefficients as in (11). For PoinCE-MC and PoinCE-der-MC, we use the sample variance as done by Roustant et al. (2020). For PoinCE-der-LARS, the total variance is obtained by the procedure detailed in section 3.4.

The upper bound to the partial variances is computed from (17) using the coefficients of the PoinCE derivative expansions as described in section 3.4.

For uniform and Gaussian input variables, the analytical expression for the Poincaré basis functions is used, while for all others, the basis functions are computed numerically using a resolution of 10^3 points for the uniform grid within the given bounds (see section 3.1).

4.1 Dyke cost model

Our first application is a simplified analytical model computing the cost associated to a dyke that is to be constructed along a stretch of river to prevent flooding (Iooss and Lemaître, 2015). Its output is the cost in million euros given by

$$Y = \mathbb{1}_{S>0} + \left[0.2 + 0.8 \left(1 - \exp^{-\frac{1000}{S^4}} \right) \right] \cdot \mathbb{1}_{S \leq 0} + \frac{1}{20} (8 \cdot \mathbb{1}_{H_d \leq 8} + H_d \cdot \mathbb{1}_{H_d > 8}) \quad (33)$$

where S is the maximal annual overflow and H_d is the dyke height. Here, the first term represents the cost of the consequences of a flooding event, the second describes the maintenance costs, and the third is associated to the construction cost. S is computed from the river characteristics detailed in Table 1 via the 1D Saint-Venant equations under several simplifying assumptions as follows:

$$S = \left(\frac{Q}{BK_s \sqrt{\frac{Z_m - Z_v}{L}}} \right)^{0.6} + Z_v - H_d - C_b \quad (34)$$

The full model has 8 input variables, of which Q , K_s , Z_v and H_d are important, and C_b , Z_m , L and B are unimportant (see also last two columns of Table 1).

The dyke cost model has been used by Roustant et al. (2020) to demonstrate the performance of projection-based PoinCE. We compare the new regression-based methods PoinCE-LARS and PoinCE-der-LARS with the projection-based counterparts PoinCE-MC and PoinCE-der-MC, and additionally with the standard PCE method PCE-LARS. The projection-based estimates use a basis of total degree 2, while the regression-based estimates use degree adaptivity with a degree of up to 5 (remember that for PoinCE, the degree corresponds to the ordering of the eigenfunctions by the magnitude of the eigenvalues). The experimental design is sampled by LHS with maximin distance optimization. For each size of the experimental design, we perform 50 independent repetitions.

Table 1: Input variables to the dyke cost model and reference values of first-order and total Sobol’ indices

Input	Function	Unit	Distribution	S_i	S_i^{tot}
Q	Maximal annual flowrate	m^3/s	Gumbel $\mathcal{G}(1013, 558)$ truncated to $[500, 3000]$	0.358	0.483
K_s	Strickler coefficient	—	Gaussian $\mathcal{N}(30, 8^2)$ truncated to $[15, +\infty]$	0.156	0.252
Z_v	River downstream level	m	Triangular $\mathcal{T}(49, 51)$	0.167	0.223
Z_m	River upstream level	m	Triangular $\mathcal{T}(54, 56)$	0.003	0.008
H_d	Dyke height	m	Uniform $\mathcal{U}([7, 9])$	0.119	0.177
C_b	Bank level	m	Triangular $\mathcal{T}(55, 56)$	0.029	0.040
L	Length of river stretch	m	Triangular $\mathcal{T}(4990, 5010)$	0.000	0.000
B	River width	m	Triangular $\mathcal{T}(295, 305)$	0.000	0.000

We show results for three input variables: the most important variable Q , the low-importance variable C_b , and the unimportant variable B . Results for the remaining input variables can be found in Appendix B.

First we investigate the two different ways to compute PoinCE: projection-based as in Roustant et al. (2020) versus sparse regression-based as described in section 3. Fig 1 and Fig. 2 show estimates for first-order and total Sobol’ indices. We observe that in all cases the regression-based estimates have a smaller variance than the corresponding projection-based estimates. Also, the median of the regression-based estimates is closer to the true Sobol’ index value than the median of the projection-based estimates. Note that while the regression-based estimates use a degree-adaptive basis of $p \leq 5$, the projection-based estimates use a fixed degree of only $p = 2$. While this choice introduces a certain bias to the projection-based estimates, a larger value for p leads to unfeasibly large variance for those estimates. This is because the coefficients of higher-order terms cannot be estimated precisely with few experimental design points, which makes the overall estimate less precise.

We also observe that regression-based estimates are often clustered around the true Sobol’ index already for very small experimental design sizes. While projection computes every coefficient independently, regression finds coefficients which jointly approximate the data as well as possible. Therefore, if an important term is missing from the expansion, projection will underestimate the true variance, while regression can somewhat compensate for the missing term by adjusting the remaining coefficients. Since regression generally leads to more precise estimates than projection, in the remainder of this paper we only show regression-based PoinCE estimates.

Furthermore, as already observed by Roustant et al. (2020), PoinCE-der estimates for Sobol’ indices have a smaller variance than PoinCE estimates. In the case of projection-based estimates, this is the case if the derivative has a smaller variance than the original model. In the case of regression, the explanation might be that PoinCE- i -der has to compute less coefficients than PoinCE for the same number of experimental design points ($\{\alpha \in \mathcal{A} : \alpha_i > 0\}$ vs. \mathcal{A}), which

can result in a more precise estimate of the true coefficient values.

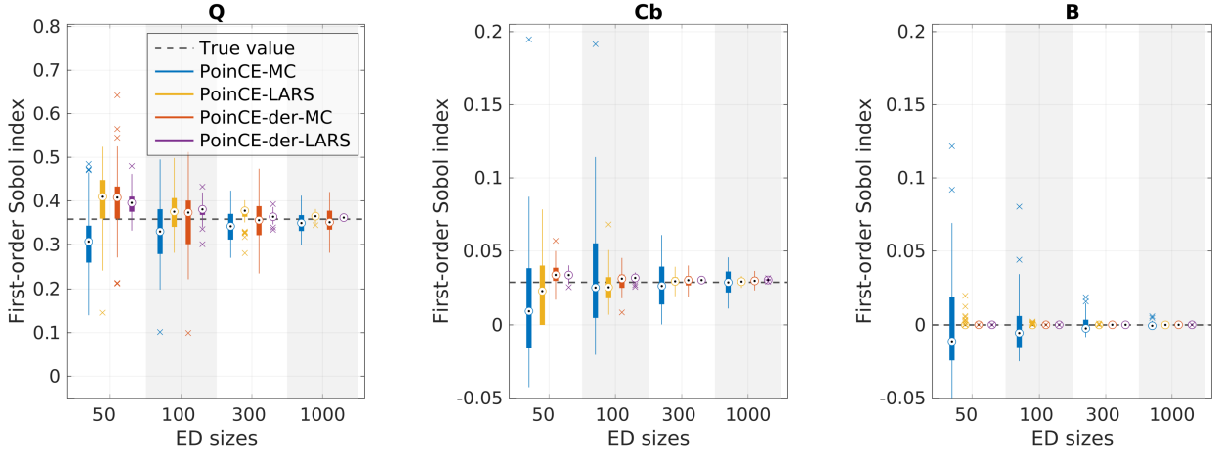


Figure 1: Comparison of PoinCE estimates of first-order Sobol' indices for the dyke cost model. Degree $p = 2$ for the MC-based estimates and $p \leq 5$ (degree-adaptive) for the regression-based estimates. Results for the remaining variables are displayed in Fig. 11 in the appendix.

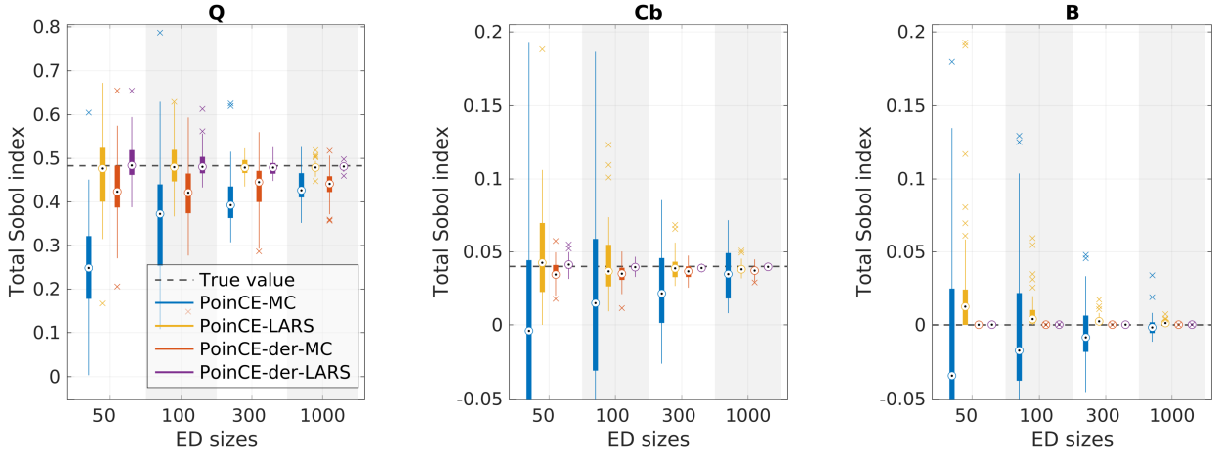


Figure 2: Comparison of PoinCE estimates of total Sobol' indices for the dyke cost model. Degree $p = 2$ for the MC-based estimates and $p \leq 5$ (degree-adaptive) for the regression-based estimates. Results for the remaining variables are displayed in Fig. 12 in the appendix.

Next, we investigate the performance of regression-based PoinCE compared to state-of-the-art PCE, and the usefulness of the DGSM-based upper bound to partial variances derived in (17). The corresponding results, unnormalized³ estimates for first-order and total Sobol' indices, are displayed in Figs. 3 and 4. Because PoinCE-der achieves more accurate estimates than PoinCE, we compute the DGSM-based upper bound using the PoinCE-der- i coefficients. For total Sobol' indices, we also include a precise Monte Carlo estimate for the DGSM-based upper bound (using 10^7 derivative samples) computed from (9) and the second inequality of (17).

We make the following observations: the PCE-LARS estimates are generally very similar to the PoinCE-LARS estimates, but the latter often have a slightly larger spread. The similarity

³We show unnormalized indices because the DGSM-based upper bound is not normalized.

might be because both rely on model evaluations only, however the respective basis functions have a very different shape (for inputs that do not follow a uniform or Gaussian distribution). In particular, the PoinCE basis functions by construction obey Neumann boundary conditions, i.e., zero derivative on the boundary.

As observed before for normalized indices, PoinCE-der performs better than PoinCE: the median is closer to the true value, and the spread is smaller. This effect is especially pronounced for low-importance variables. In 8 dimensions, a PoinCE-der expansion of degree 5 has 495 terms while the total-degree basis of PCE and PDO has 1287 terms, which means that a PoinCE-der expansion has to estimate less than half of the coefficients. PoinCE-der generally gives a tighter “lower bound” than PCE (but note that the estimates are not guaranteed to be a lower bound).

By definition, the DGSM-based upper bound estimate is larger than or equal to the corresponding total Sobol’ index estimate. However it is a true upper bound only when the full infinite expansion is used. This is visible in Figs. 4 and 14: for some inputs, the upper bound estimate almost coincides with the Sobol’ index estimate, and is smaller than the true Sobol’ index.

For other inputs, such as K_s and especially H_d (see Fig. 14), the DGSM-based upper bound is very loose. An explanation for the large gap between the lower and upper bound for H_d might be that H_d is responsible for a kink in the model (through the last term of (33)) which is difficult to approximate by differentiable functions. Therefore, its expansion needs high-order terms. From (17) it follows that even if the PoinCE finds the true coefficients, the upper bound is very loose due to the quickly-growing eigenvalues.

Finally, we see that in many cases the gap between the upper bound estimate and its true value is larger than the gap between Sobol’ index estimate and its true value. The reason might be that some higher-order terms are still missing from the considered expansion. Due to the eigenvalue factor involved in the estimate of the upper bound (17), this has a larger influence on the upper bound than on the Sobol’ index estimate.

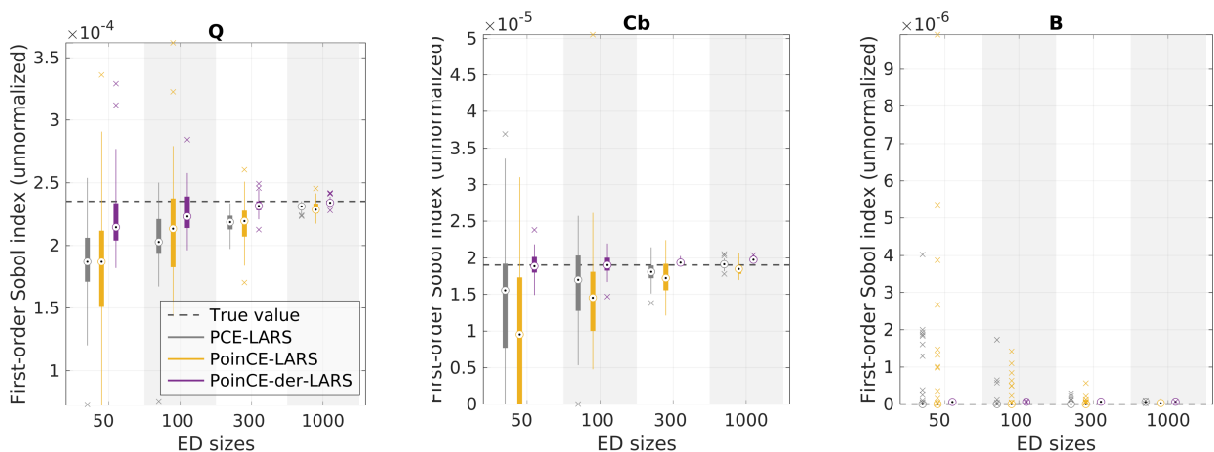


Figure 3: Estimates of unnormalized first-order Sobol’ indices for the dyke cost model ($p \leq 5$). Boxplots: in grey the PCE-based estimates and in black the DGSM-based upper bound from (17). The dashed line denotes a high-precision estimate for the unnormalized first-order Sobol’ index. Results for the remaining input variables can be found in Fig. 13 in the appendix.

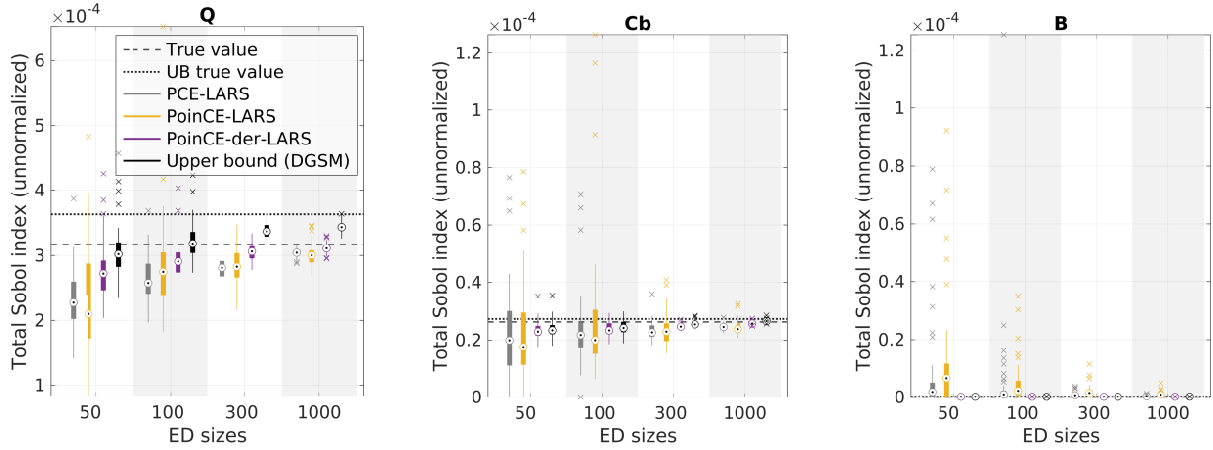


Figure 4: Estimates of unnormalized total Sobol' indices for the dyke cost model ($p \leq 5$). Boxplots: in grey the PCE-based estimates and in black the DGSM-based upper bound from (17). Lines: the dashed line denotes a high-precision estimate for the unnormalized total Sobol' index, while the dotted line is a MC-based high-precision estimate for the DGSM-based upper bound. Results for the remaining input variables can be found in Fig. 14 in the appendix.

To estimate Sobol' indices precisely, it is crucial to have a good estimate for the total variance. For PCE-LARS, PoinCE-LARS, and PoinCE-der-LARS, this value can directly be computed from the expansion coefficients, while for PoinCE computed by projection, we are using the empirical variance, as detailed in the beginning of section 4. In Fig. 5a we display the scatter of the variance estimates (50 replications). The empirical estimate has the largest variation, while PoinCE-der-LARS has the smallest. PCE-LARS and PoinCE-LARS underestimate the total variance more than PoinCE-der-LARS. This is likely one reason for the good performance of PoinCE-der for the estimation of Sobol' indices: a more accurate total variance leads to more accurate Sobol' indices.

Interestingly, while PoinCE performs well for the estimation of Sobol' indices, the same is not true for the generalization error, given by the relative mean-squared error

$$\text{RelMSE} = \frac{\mathbb{E}_X [(f(X) - f^{\text{surr}}(X))^2]}{\text{Var}_X [f(X)]} \quad (35)$$

with the surrogate model f^{surr} . The RelMSE is computed by Monte Carlo integration on a validation set of size 10^6 sampled from the input distribution μ . In Fig. 5b we display boxplots of estimates for the generalization error on a validation set of size 10^6 (mean-squared error normalized by the variance of the validation set). While PoinCE-der performs better than PoinCE, PCE has an even smaller relative MSE and shows faster convergence behavior. PoinCE-der performs better than PCE only for very small experimental design sizes.

Finally, we display the number of nonzero coefficients of each expansion in Fig. 5c. PCE and PoinCE have a similar number of active coefficients, while PoinCE-der has considerably more active coefficients. This corresponds to a better validation error only for the smallest experimental design size (Fig. 5b). A possible explanation is the following: using the derivative information to compute PoinCE-der, the same amount of data is used for a (truncated) expansion containing

less terms than the PoinCE expansion has (since some terms, which do not contain the variable for which the partial derivative is taken, drop out). In this way, more coefficients can be computed.

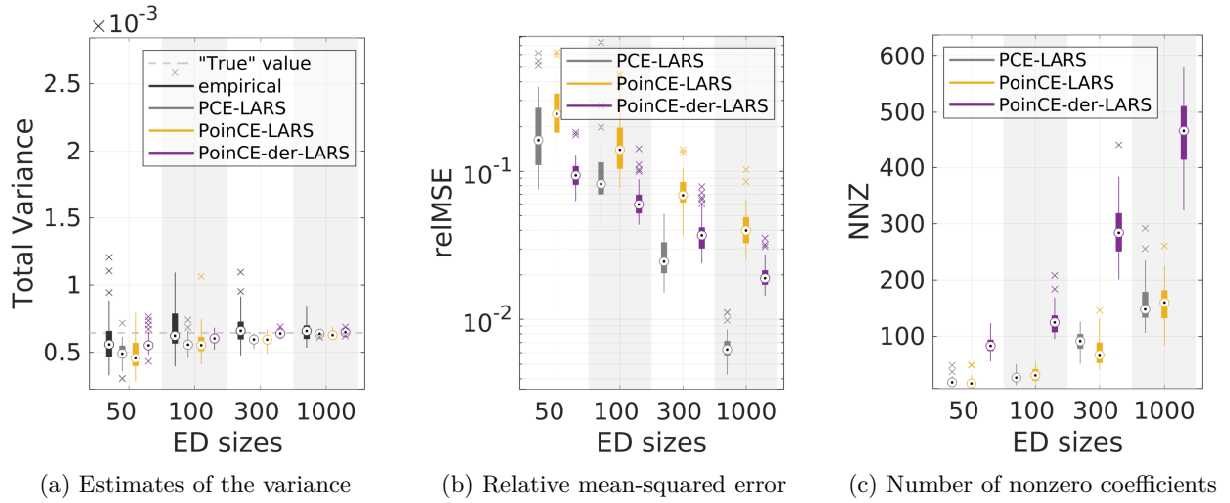


Figure 5: Dyke cost model: Comparison of PCE and PoinCE(-der) with respect to the following metrics: estimation of total variance, relative mean-squared error, and number of nonzero coefficients in the respective expansions.

4.2 Mascaret data set

Our second application focuses on a phenomenological and industrial simulation model, called Mascaret (Goutal et al., 2012), based on a 1D solver of the Saint Venant equations and aiming at computing water height for river flood events. The studied case, taken from Petit et al. (2016) and also studied in Roustant et al. (2017), is the French Vienne river in permanent regime whose uncertain input data concern flowrate, several physical parameters and geometrical data (transverse river profiles). 37 independent inputs have then been considered as random variables:

- 12 Strickler coefficients of the main channel $K_{s,c}^i$, uniform in $[20, 40]$;
- 12 Strickler coefficients of the flood plain $K_{s,p}^i$, uniform in $[10, 30]$;
- 12 slope perturbations dZ^i , standard Gaussian with bounds $[-3, 3]$;
- 1 discharge value Q , Gaussian with zero mean and standard deviation 50, bounds $[-150, 50]$.

The derivatives of the model output with respect to these 37 inputs have been efficiently (with a cost independent of the number of inputs) computed by using the adjoint model of Mascaret obtained by automatic differentiation (Griewank and Walther, 2008). A large-size Monte Carlo sample ($n = 20\,000$) is available from the study of Petit et al. (2016). This data set contains all the values of the 37 inputs, the water height as output and the 37 partial derivatives of the output (one derivative with respect to each input). Note that this sample, which has a very large size, has been obtained during a research work for a demonstrative purpose. In industrial

practice, the aim is to use the minimal possible sample size: it is expected to use methods able to deal with sample sizes of the order of one hundred.

Previous studies on this data set (Petit et al., 2016; Roustant et al., 2017) have identified 32 of the 37 inputs as noninfluential. In our study, we display results for the 5 remaining inputs ($K_{s,c}^{11}$, $K_{s,c}^{12}$, dZ^{11} , dZ^{12} , and Q) and for one of the noninfluential inputs ($K_{s,c}^1$). We choose a basis with hyperbolic truncation using $q = 0.5$, and degree adaptivity $p = 1, 2, \dots, 8$. We analyze several experimental design sizes ranging from 30 to 300. For each experimental design size, we run 30 replications, sampling the design randomly without replacement from the given full data set. “True” values for Sobol’ indices and total variance are computed from a PCE using all 20 000 points.

Estimates of first-order and total Sobol’ indices are displayed in Figs. 6 and 7. We display results for regression-based PCE, PoinCE, and PoinCE-der. In addition, we display the upper bound computed as in (17), computed based on PoinCE-der coefficients and normalized by the PoinCE-der total variance. We observe that for the non-influential variable $K_{s,c}^1$ (and indeed all other 31 non-influential variables), derivative-based PoinCE correctly identify a total and first-order Sobol’ index of 0. Overall, PoinCE and PCE show very similar results, with PoinCE having slightly larger variance in a few cases. For some variables such as dZ^{11} and Q , the DGSM upper bound almost coincides with the PoinCE-der estimate. Overall, we observe that PoinCE-der estimates have smaller variance than PCE and PoinCE for the important variables $K_{s,c}^{11}$, dZ^{11} , and Q , even already for 30 experimental design points. For low-importance variables such as $K_{s,c}^{12}$ and dZ^{12} , PoinCE-der correctly identifies a value away from zero already for the smallest experimental design, while half of the PCE and PoinCE estimates are zero. For small experimental design sizes, the PoinCE-der estimates also have a smaller bias than the PCE and PoinCE estimates. Sometimes the PoinCE-der estimates seem to systematically over- or underestimate the true Sobol’ index by a small amount. However note that the “true” value was computed by a PCE (based on all 20 000 points), and might therefore itself be slightly inaccurate.

In Fig. 8a we display various estimates for the total variance. We observe again that PoinCE-der yields an estimate with smaller variance and less bias than PoinCE and PCE. PoinCE and PCE both have smaller variance than the empirical estimate, but generally underestimate the total variance. While PoinCE-der estimates Sobol’ indices and total variance well, we observe in Fig. 8b showing the relative MSE that PCE and PoinCE are performing better as global surrogate models: their model approximation error is for large experimental designs almost an order of magnitude better than for PoinCE-der.

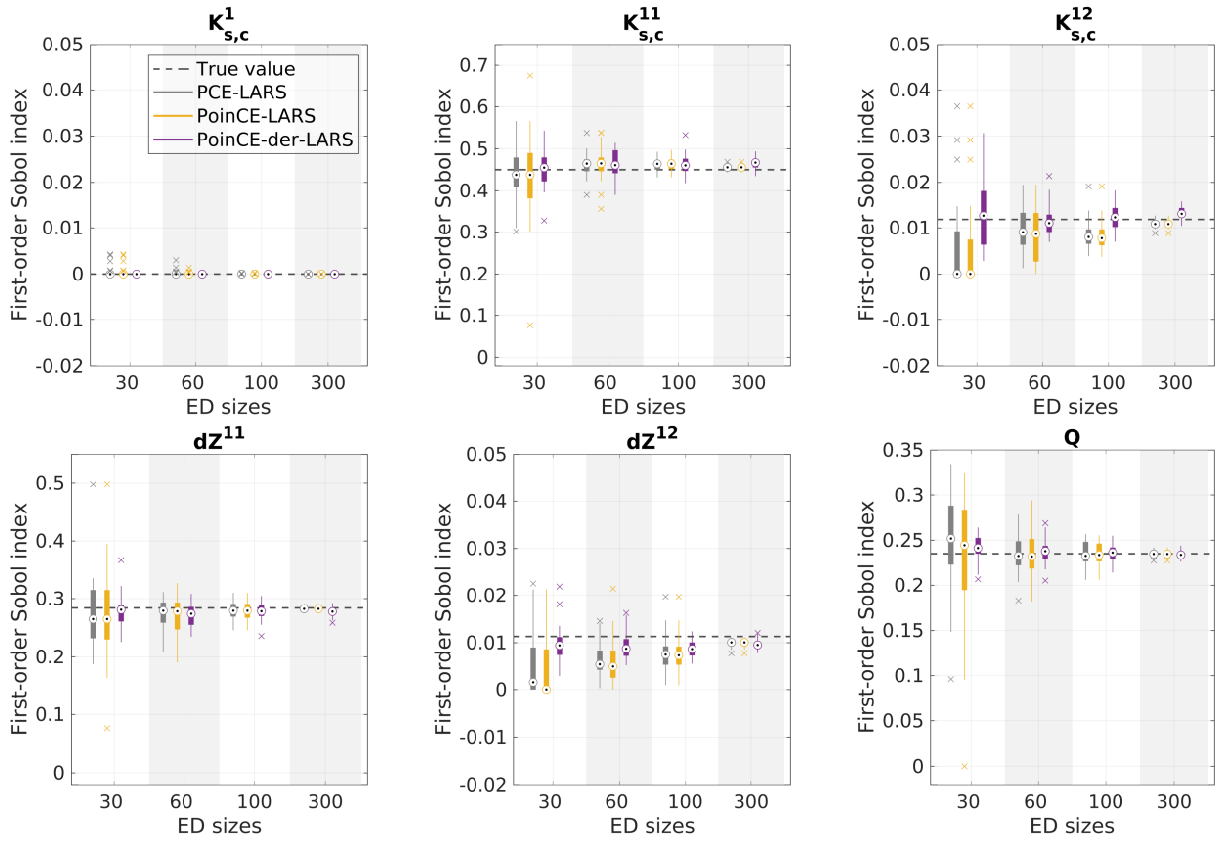


Figure 6: First-order Sobol' indices for the Mascaret data set (30 replications). “True” values computed from a PCE using all 20 000 points.

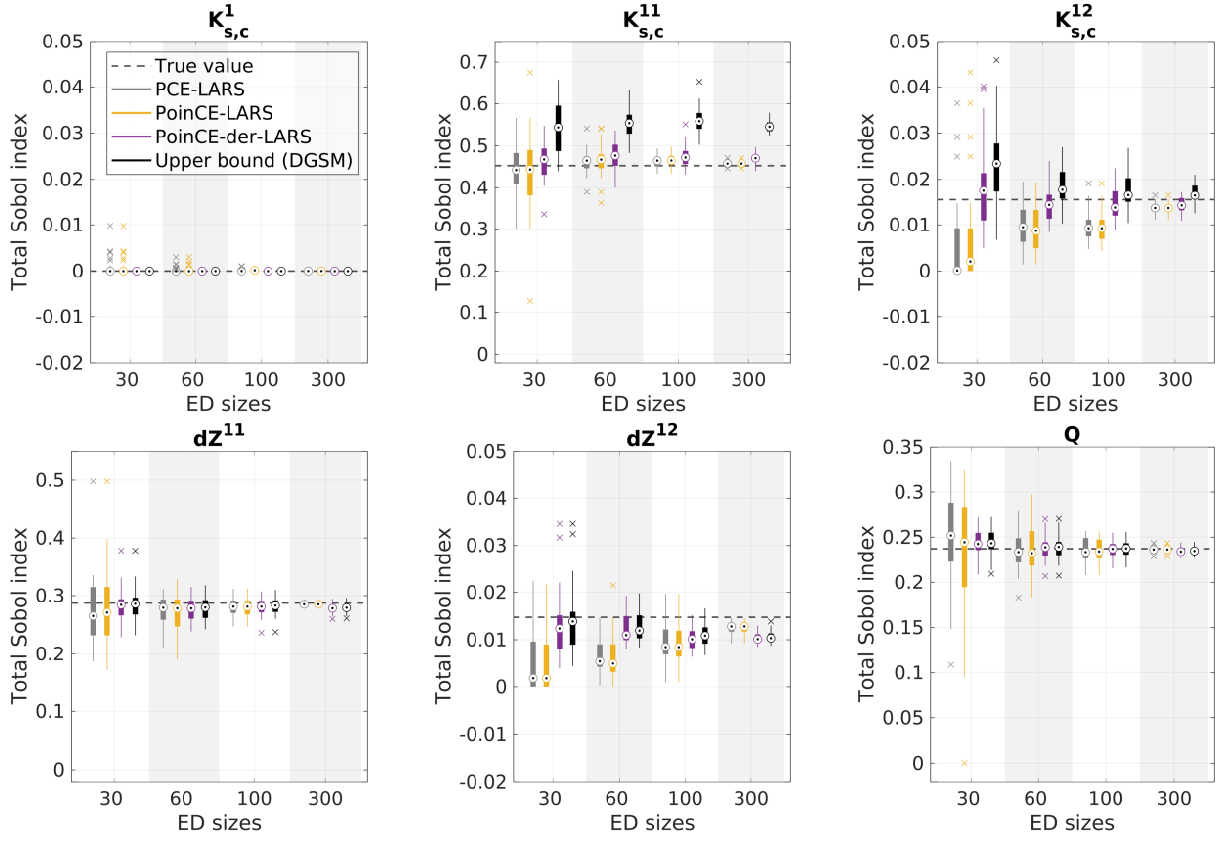


Figure 7: Total Sobol' indices for the Mascaret data set (30 replications). “True” values computed from a PCE using all 20 000 points.

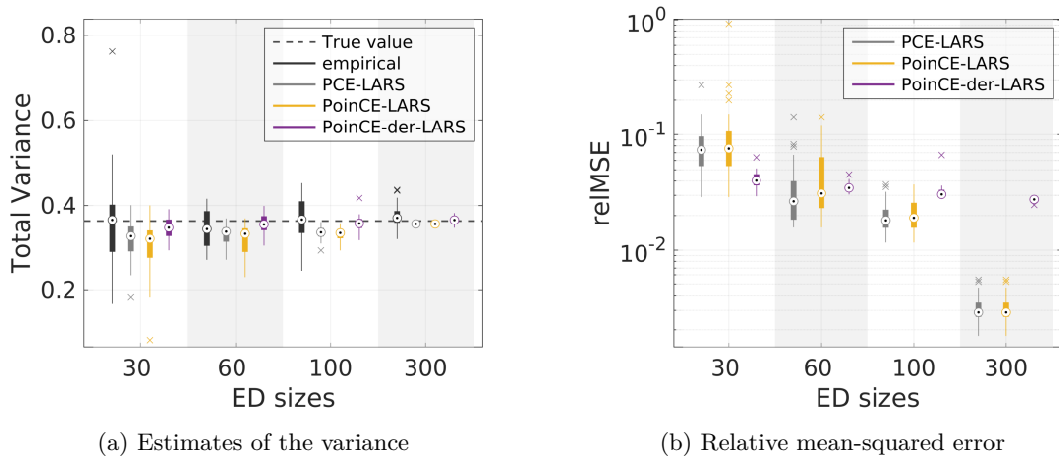


Figure 8: Mascaret data set. Comparison of PCE and PoinCE(-der) with respect to the following metrics: estimation of total variance, and relative mean-squared error. “True” value of total variance computed from a PCE using all 20 000 points.

5 Conclusion

In this paper we studied PoinCE, an expansion in terms of the Poincaré basis, which is an orthonormal basis of $L^2(\mu)$ with the unique property that all its partial derivatives form again an orthogonal basis for the same space. We provided a proof of this property as well as a few analytical results as direct consequences. In particular, we showed how upper and lower bounds for partial variances can be obtained analytically from PoinCE coefficients.

We described the computation of PoinCE and Poincaré derivative expansions by sparse regression and applied the method to two numerical examples. We found that while PoinCE does not outperform PCE in terms of validation error, it can be advantageous for estimating Sobol’ indices in the low-data regime. PoinCE is therefore a valuable tool if model derivatives are cheaply available (e.g., by automatic differentiation or as a by-product of the simulation). Taking partial derivatives reduces the size of the truncated basis especially for high-dimensional, low-order total-degree bases, which gives an advantage to derivative-based PoinCE over expansions relying on model evaluations.

Future work on the topic of PoinCE will investigate the simultaneous use of model evaluations and derivatives for the computation of the coefficients, and compare to the related topic of gradient-enhanced PCE.

Acknowledgments

This paper is a part of the project “Surrogate Modeling for Stochastic Simulators (SAMOS)” funded by the Swiss National Science Foundation (Grant #200021_175524), whose support is gratefully acknowledged. Part of this research was conducted within the frame of the Chair in Applied Mathematics OQUAIDO, gathering partners in technological research (BRGM, CEA, IFPEN, IRSN, Safran, Storengy) and academia (CNRS, Ecole Centrale de Lyon, Mines Saint-Etienne, University of Grenoble, University of Nice, University of Toulouse) around advanced methods for ComputerExperiments. Support from the ANR-3IA Artificial and Natural Intelligence Toulouse Institute is gratefully acknowledged.

References

- Anderson, G. W., A. Guionnet, and O. Zeitouni (2010). *An introduction to random matrices*. Number 118. Cambridge University Press.
- Bakry, D., I. Gentil, and M. Ledoux (2014). *Analysis and geometry of Markov diffusion operators, volume 348 of Grundlehren der Mathematischen Wissenschaften [Fundamental Principles of Mathematical Sciences]*. Springer, Cham.
- Blatman, G. and B. Sudret (2008). Sparse polynomial chaos expansions and adaptive stochastic finite elements using a regression approach. *Comptes Rendus Mécanique* 336(6), 518–523.

- Blatman, G. and B. Sudret (2011). Adaptive sparse polynomial chaos expansion based on least angle regression. *Journal of Computational Physics* 230, 2345–2367.
- Borgonovo, E. and E. Plischke (2016). Sensitivity analysis: A review of recent advances. *European Journal of Operational Research* 248, 869–887.
- Candès, E. J. and Y. Plan (2011). A probabilistic and RIPless theory of compressed sensing. *IEEE Transactions on Information Theory* 57(11), 7235–7254.
- Chapelle, O., V. Vapnik, and Y. Bengio (2002). Model selection for small sample regression. *Machine Learning* 48(1), 9–23.
- Efron, B. and C. Stein (1981). The jackknife estimate of variance. *The Annals of Statistics* 9, 586–596.
- Ernst, O., A. Mugler, H.-J. Starkloff, and E. Ullmann (2012). On the convergence of generalized polynomial chaos expansions. *ESAIM: Mathematical Modelling and Numerical Analysis* 46(02), 317–339.
- Fang, K.-T., R. Li, and A. Sudjianto (2006). *Design and modeling for computer experiments*. Chapman & Hall/CRC.
- Gejadzea, I., P.-O. Malaterre, and V. Shutyaev (2019). On the use of derivatives in the polynomial chaos based global sensitivity and uncertainty analysis applied to the distributed parameter models. *Journal of Computational Physics* 381, 218–245.
- Gerstner, T. and M. Griebel (1998). Numerical integration using sparse grids. *Numerical algorithms* 18(3), 209–232.
- Ghanem, R. and P. Spanos (1990). Polynomial chaos in stochastic finite elements. *Journal of Applied Mechanics* 57(1), 197–202.
- Ghanem, R. G. and P. Spanos (1991). *Stochastic finite elements – A spectral approach*. Springer Verlag, New York. (Reedited by Dover Publications, Mineola, 2003).
- Goutal, N., J.-M. Lacombe, F. Zaoui, and K. El-Kadi-Abderrezak (2012, september). MAS-CARET: a 1-D open-source software for flow hydrodynamic and water quality in open channel networks. In R. Murillo Muñoz (Ed.), *River Flow 2012: Proceedings of the International Conference on Fluvial Hydraulics*, Volume 2, San José, Costa Rica, pp. 1169–1174. CRC Press.
- Griewank, A. and A. Walther (2008). *Evaluating derivatives: Principles and techniques of automatic differentiation*. SIAM Philadelphia.
- Guo, L., A. Narayan, and T. Zhou (2018). A gradient enhanced ℓ^1 -minimization for sparse approximation of polynomial chaos expansions. *Journal of Computational Physics*. 367, 49–64.
- Hoeffding, W. (1948). A class of statistics with asymptotically normal distributions. *Annals of Mathematical Statistics* 19, 293–325.

- Homma, T. and A. Saltelli (1996). Importance measures in global sensitivity analysis of non linear models. *Reliability Engineering & System Safety* 52, 1–17.
- Iooss, B. and P. Lemaître (2015). A review on global sensitivity analysis methods. In C. Meloni and G. Dellino (Eds.), *Uncertainty management in Simulation-Optimization of Complex Systems: Algorithms and Applications*, pp. 101–122. Springer.
- Jakeman, J. D., M. S. Eldred, and K. Sargsyan (2015). Enhancing ℓ_1 -minimization estimates of polynomial chaos expansions using basis selection. *Journal of Computational Physics*. 289, 18–34.
- Keese, A. and H. G. Matthies (2003). Sparse quadrature as an alternative to monte carlo for stochastic finite element techniques. In *PAMM: Proceedings in Applied Mathematics and Mechanics*, Volume 3, pp. 493–494. Wiley Online Library.
- Knio, O. M. and O. Le Maitre (2006). Uncertainty propagation in CFD using polynomial chaos decomposition. *Fluid dynamics research* 38(9), 616.
- Kucherenko, S. and B. Iooss (2017). Derivative-based global sensitivity measures. In R. Ghanem, D. Higdon, and H. Owhadi (Eds.), *Springer Handbook on Uncertainty Quantification*, pp. 1241–1263. Springer.
- Lamboni, M., B. Iooss, A.-L. Popelin, and F. Gamboa (2013). Derivative-based global sensitivity measures: General links with Sobol’ indices and numerical tests. *Mathematics and Computers in Simulation* 87, 45–54.
- Le Gratiet, L., S. Marelli, and B. Sudret (2017). Metamodel-based sensitivity analysis: Polynomial chaos expansions and Gaussian processes. In R. Ghanem, D. Higdon, and H. Owhadi (Eds.), *Springer Handbook on Uncertainty Quantification*, pp. 1289–1325. Springer.
- Li, Y., M. Anitescu, O. Roderick, and F. Hickernell (2011). Orthogonal bases for polynomial regression with derivative information in uncertainty quantification. *International Journal for Uncertainty Quantification* 1, 297–320.
- Lüthen, N., S. Marelli, and B. Sudret (2021a). A benchmark of basis-adaptive sparse polynomial chaos expansions for engineering regression problems. *Int. J. Uncertainty Quantification*. (submitted).
- Lüthen, N., S. Marelli, and B. Sudret (2021b). Sparse polynomial chaos expansions: Literature survey and benchmark. *SIAM/ASA Journal on Uncertainty Quantification* 9(2), 593–649.
- Marelli, S., N. Lüthen, and B. Sudret (2021). UQLab user manual – Polynomial chaos expansions. Technical report, Chair of Risk, Safety and Uncertainty Quantification, ETH Zurich, Switzerland. Report # UQLab-V1.4-104.
- Marelli, S. and B. Sudret (2014). UQLab: A framework for uncertainty quantification in Matlab. In *Vulnerability, Uncertainty, and Risk (Proc. 2nd Int. Conf. on Vulnerability, Risk Analysis and Management (ICVRAM2014), Liverpool, United Kingdom)*, pp. 2554–2563.

- McKay, M. D., R. J. Beckman, and W. J. Conover (1979). A comparison of three methods for selecting values of input variables in the analysis of output from a computer code. *Technometrics* 2, 239–245.
- Mikolas, M. (1955). über gewisse Eigenschaften orthogonaler Systeme der Klasse L^2 und die Eigenfunktionen Sturm-Liouvillescher Differentialgleichungen. *Acta Mathematica Academiae Scientiarum Hungaricae* 6, 147–190.
- Oladyshkin, S. and W. Nowak (2012). Data-driven uncertainty quantification using the arbitrary polynomial chaos expansion. *Reliab. Eng. Sys. Safety* 106, 179–190.
- Peng, J., J. Hampton, and A. Doostan (2016). On polynomial chaos expansion via gradient-enhanced l_1 -minimization. *Journal of Computational Physics* 310, 440–458.
- Petit, S., F. Zaoui, A.-L. Popelin, C. Goeury, and N. Goutal (2016). Couplage entre indices à base de dérivées et mode adjoint pour l’analyse de sensibilité globale. Application sur le code Mascaret. Preprint, <https://hal.archives-ouvertes.fr/hal-01373535>.
- Prieur, C. and S. Tarantola (2017). Variance-based sensitivity analysis: Theory and estimation algorithms. In R. Ghanem, D. Higdon, and H. Owhadi (Eds.), *Springer Handbook on Uncertainty Quantification*, pp. 1217–1239. Springer.
- Razavi, S., A. Jakeman, A. Saltelli, C. Prieur, B. Iooss, E. Borgonovo, E. Plischke, S. Lo Piano, T. Iwanaga, W. Becker, S. Tarantola, J. Guillaume, J. Jakeman, H. Gupta, N. Melillo, G. Rabbiti, V. Chabridon, Q. Duan, X. Sun, S. Smith, R. Sheikholeslami, N. Hosseini, M. Asadzadeh, A. Puy, S. Kucherenko, and H. Maier (2021). The future of sensitivity analysis: An essential discipline for systems modelling and policy making. *Environmental Modelling and Software* 137(104954).
- Roderick, O., M. Anitescu, and P. Fischer (2010). Polynomial regression approaches using derivative information for uncertainty quantification. *Nuclear Science and Engineering* 164, 122–139.
- Roustant, O., F. Barthe, and B. Iooss (2017). Poincaré inequalities on intervals - application to sensitivity analysis. *Electronic Journal of Statistics* 2, 3081–3119.
- Roustant, O., F. Gamboa, and B. Iooss (2020). Parseval inequalities and lower bounds for variance-based sensitivity indices. *Electronic Journal of Statistics* 14, 386–412.
- Simon, B. (2010). *Szegő’s theorem and its descendants: spectral theory for L^2 perturbations of orthogonal polynomials*. Princeton University Press.
- Smith, R. (2014). *Uncertainty quantification*. SIAM.
- Sobol’, I. (1993). Sensitivity estimates for non linear mathematical models. *Mathematical Modelling and Computational Experiments* 1, 407–414.

- Sobol, I. and A. Gresham (1995). On an alternative global sensitivity estimators. In *Proceedings of SAMO 1995*, Belgirate, pp. 40–42.
- Sudret, B. (2006). Global sensitivity analysis using polynomial chaos expansions. In P. Spanos and G. Deodatis (Eds.), *Proc. 5th Int. Conf. on Comp. Stoch. Mech (CSM5)*, Rhodes, Greece, June 21-23.
- Sudret, B. (2008). Global sensitivity analysis using polynomial chaos expansion. *Reliability Engineering & System Safety* 93, 964–979.
- Sudret, B. and C.-V. Mai (2015). Computing derivative-based global sensitivity measures using polynomial chaos expansions. *Reliability Engineering & System Safety* 134, 241–250.
- Szegő, G. (1939). *Orthogonal polynomials*, Volume 23. American Mathematical Soc.
- Torre, E., S. Marelli, P. Embrechts, and B. Sudret (2019). Data-driven polynomial chaos expansion for machine learning regression. *Journal of Computational Physics* 388, 601–623.
- Wiener, N. (1938). The homogeneous chaos. *American Journal of Mathematics* 60, 897–936.
- Zettl, A. (2010). *Sturm-Liouville theory*. Number 121. American Mathematical Society.

A Triangular distribution

The triangular distribution has one non-differentiable point at its mode. It is therefore only in class C^0 , and its eigenfunctions are in class C^1 (Roustant et al., 2017, Theorem 2). Our computation procedure described in section 3 uses linear FEM on a uniform grid with 1000 points in the rescaled space where the support of the triangular distribution is $[-1, 1]$. As a second step, to facilitate the computation of continuous basis derivatives, the eigenvectors obtained by FEM are interpolated by cubic splines with zero derivatives at the boundary. However, cubic splines are in class C^2 but the eigenfunctions of the triangular distribution only in class C^1 . To assert that this procedure does not lead to overly smooth eigenfunction approximations for the triangular distribution, we study the convergence for increasingly fine meshes (since inaccuracies should be local and decrease with increasingly fine meshsize). If there is no significant change in basis functions or Sobol' indices from our refinement (1000 points) to a $10\times$ or $100\times$ finer one, then we can consider the numerical procedure accurate enough.

In Figure 9 we display the first few Poincaré basis functions and derivatives of the triangular distribution for a FE mesh with 10^3 points (as in section 4) and for a mesh with 10^5 points (i.e., 100 times finer). There is no visible difference between the respective basis functions and derivatives on the different refinement levels. The $L^2(\mu)$ -error between the basis function and basis derivative approximations is in $\mathcal{O}(10^{-9})$.

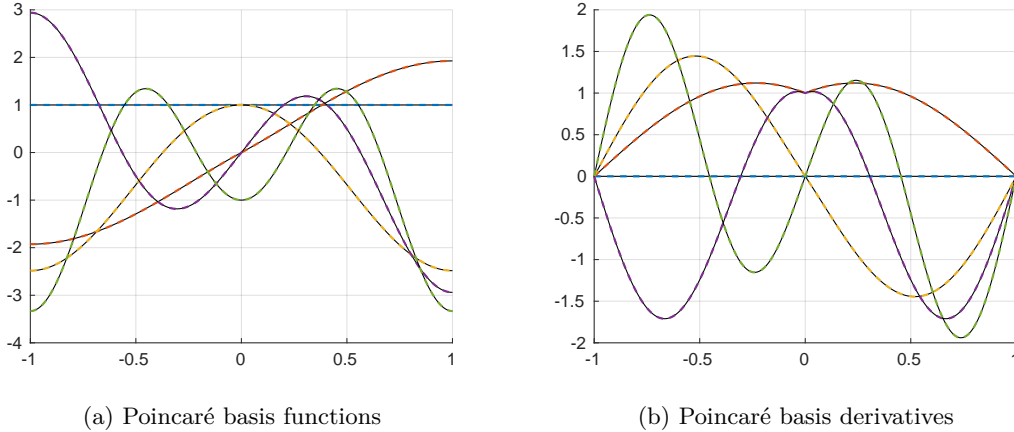


Figure 9: First few Poincaré basis functions and their derivatives of the triangular distribution. Black lines: functions computed on a FE mesh with 10^5 points. Colorful dashed lines: functions computed on a FE mesh with 10^3 points.

In Table 2 we show exemplary results for the dyke cost model (section 4.1) and a fixed experimental design of 100 points. The dyke cost model has 5 triangular variables (see Table 1). We compute the eigenfunctions once with a uniform FE mesh of 10^3 points, as in section 4, and then with 10^4 points, and we compare the resulting Sobol' indices. We observe that the absolute difference is in $\mathcal{O}(10^{-5})$, well below the accuracy of the given analytical values (Table 1). (The absolute differences for the same quantities between a mesh of 10^2 vs 10^3 points are at most 10^{-3} .)

Table 2: Absolute difference between Sobol’ index estimates when using a FE mesh with 10^3 vs 10^4 points, for the dyke cost model and a specific experimental design with 100 points

Input	PoinCE, Total	PoinCE, First-order	PoinCE-der, Total	PoinCE-der, First-order
Q	7.39e-08	2.44e-07	4.49e-07	1.06e-07
K_s	4.73e-07	2.67e-07	6.80e-06	9.25e-07
Z_v	1.33e-07	2.39e-07	4.78e-07	1.09e-07
Z_m	4.94e-08	2.00e-08	6.52e-09	5.41e-09
H_d	2.50e-07	1.94e-07	2.21e-07	5.88e-08
C_b	1.04e-07	3.12e-08	6.91e-08	4.74e-08
L	1.09e-07	0.00e+00	6.74e-14	5.53e-13
B	4.61e-09	0.00e+00	1.15e-10	7.55e-11

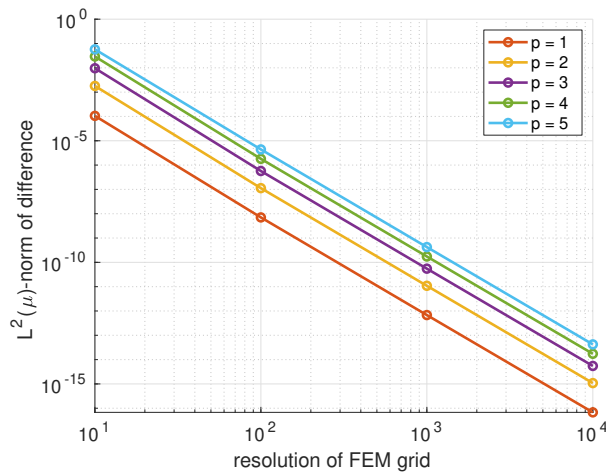


Figure 10: Convergence of the first few Poincaré basis functions for the uniform distribution

For the uniform distribution, the Poincaré basis is known analytically. The convergence of the first few basis functions, measured in the $L^2(\mu)$ -norm of the difference between the numerical and the analytical eigenfunctions, is shown in Fig. 10 for an increasingly fine FE mesh. We clearly observe an exponential decay of the error. The eigenfunction of degree 0 is not shown in the plot because it is constant and therefore approximated without any error.

B Additional results

In Figs. 11-14, we show additional results for the dyke cost model, namely Sobol’ index estimates (normalized and unnormalized) for the remaining five input dimensions. For the corresponding discussion, see section 4.1.

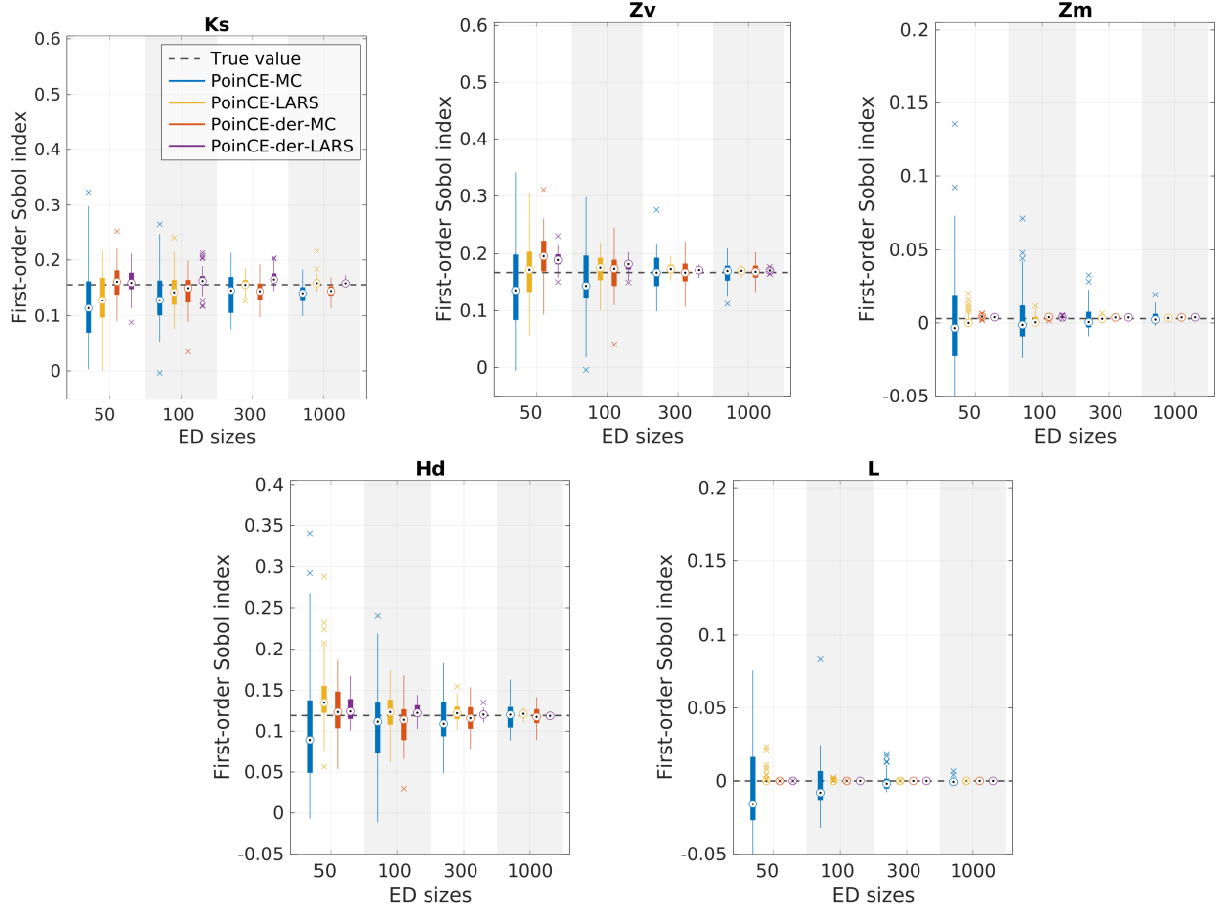


Figure 11: Comparison of PoinCE estimates of first-order Sobol' indices for the dyke cost model. Degree $p = 2$ for the MC-based estimates and $p \leq 5$ (degree-adaptive) for the regression-based estimates. See also Fig. 1 in the main part of the paper.

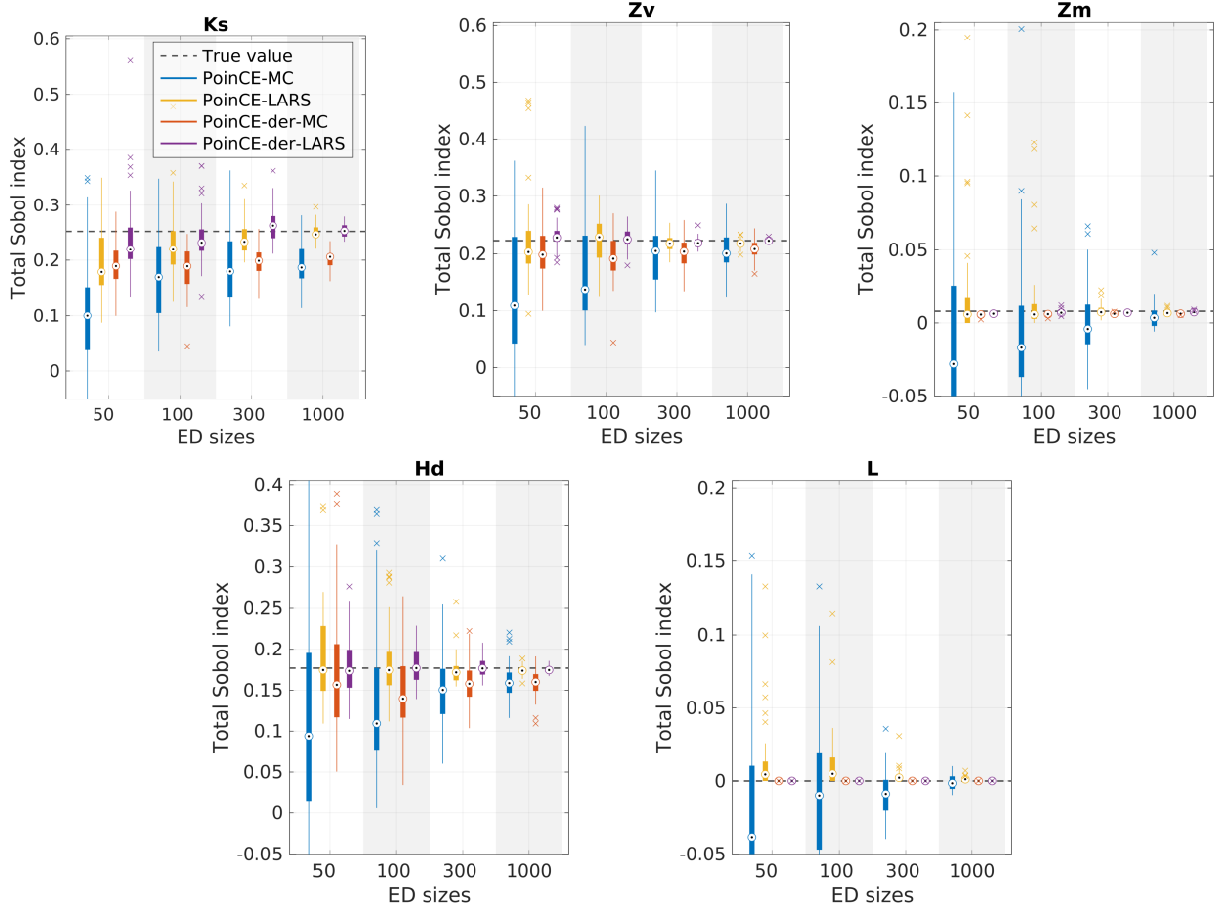


Figure 12: Comparison of PoinCE estimates of total Sobol' indices for the dyke cost model. Degree $p = 2$ for the MC-based estimates and $p \leq 5$ (degree-adaptive) for the regression-based estimates. See also Fig. 2 in the main part of the paper.

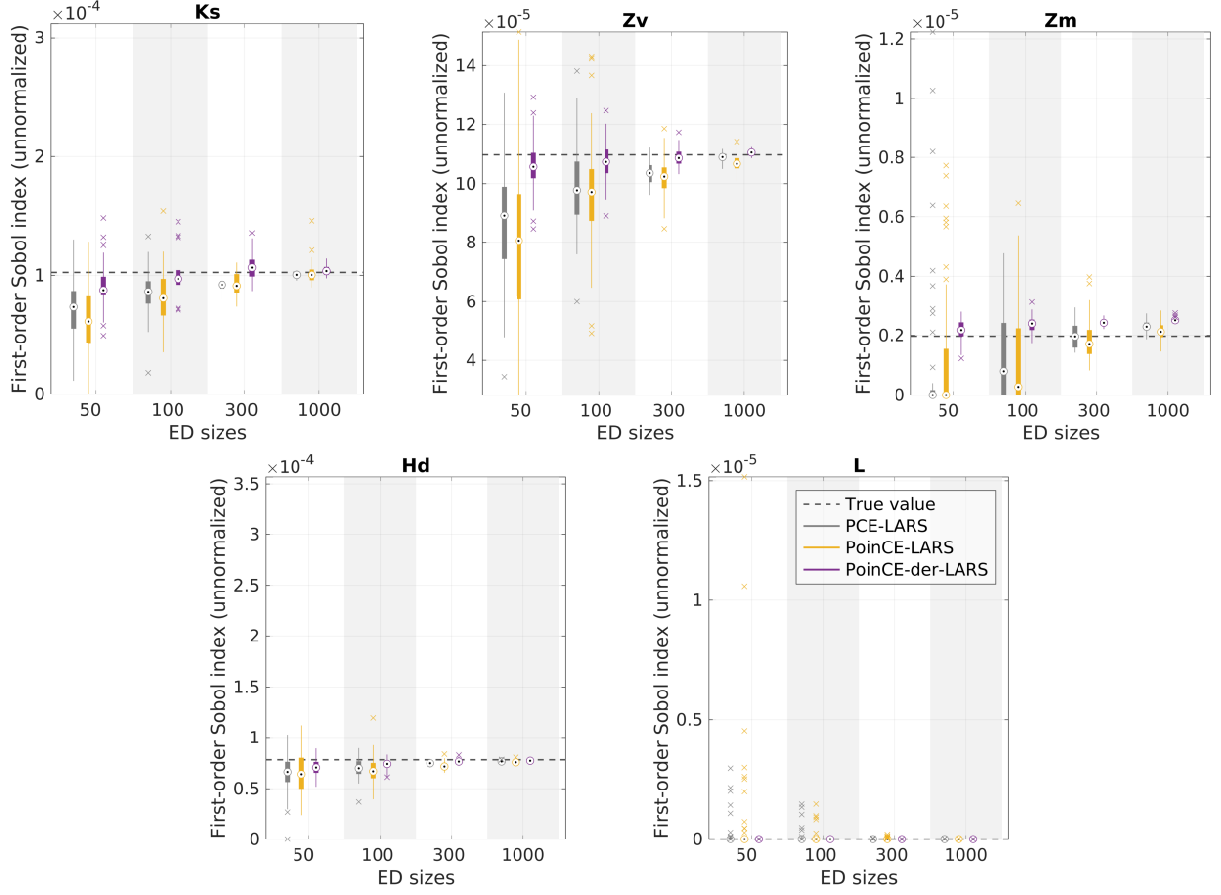


Figure 13: Estimates of unnormalized first-order Sobol' indices for the dyke cost model ($p \leq 5$). Boxplots: in grey the PCE-based estimates and in black the DGSM-based upper bound from (17). The dashed line denotes a high-precision estimate for the unnormalized first-order Sobol' index. See also Fig. 3.

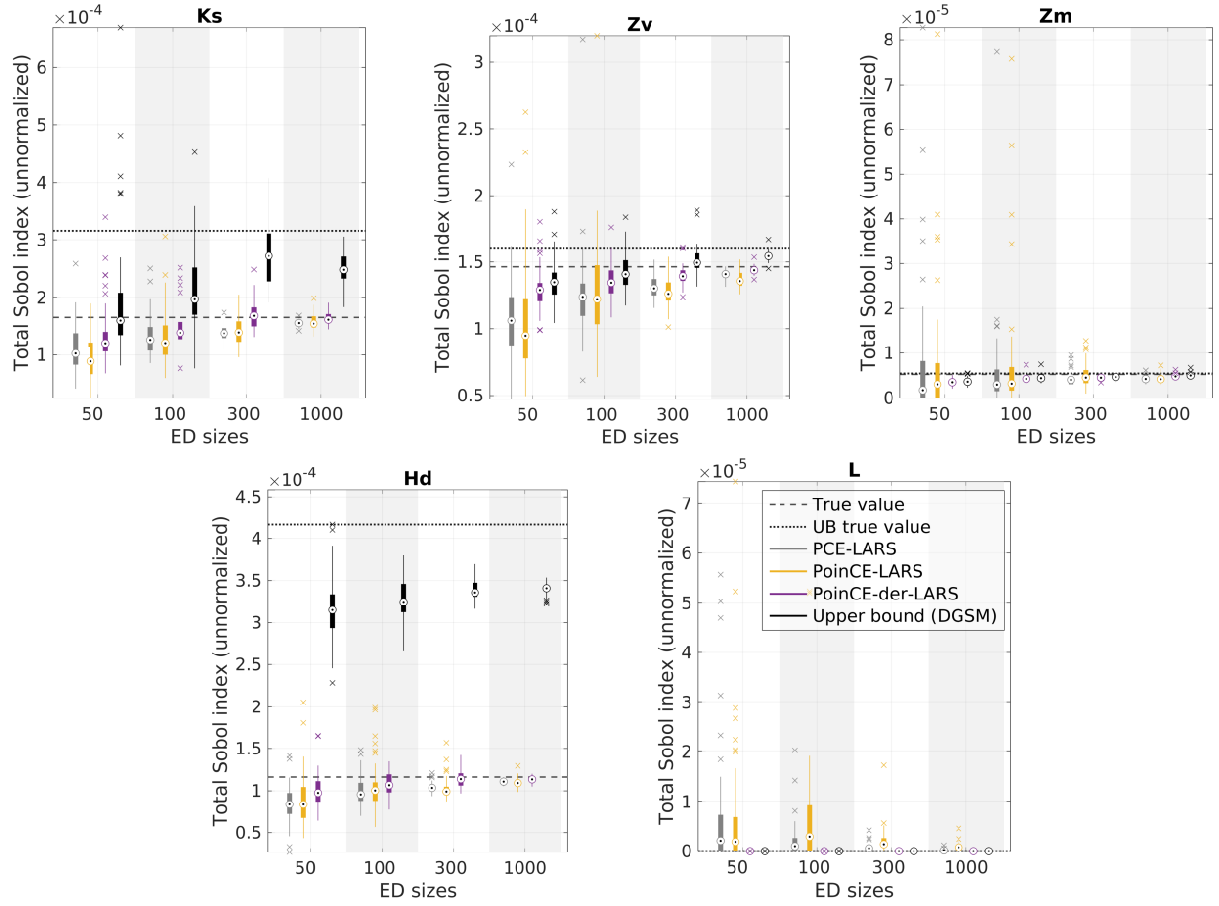


Figure 14: Estimates of unnormalized total Sobol' indices for the dyke cost model ($p \leq 5$). Boxplots: in grey the PCE-based estimates and in black the DGSM-based upper bound from (17). Lines: the dashed line denotes a high-precision estimate for the unnormalized total Sobol' index, while the dotted line is a MC-based high-precision estimate for the DGSM-based upper bound. See also Fig. 4.